

# Average observational quantities in the timescape cosmology

David L. Wiltshire\*

*Department of Physics & Astronomy, University of Canterbury,  
Private Bag 4800, Christchurch 8140, New Zealand<sup>†</sup>; and*

*International Center for Relativistic Astrophysics Network (ICRANet), P.le della Repubblica 10, Pescara 65121, Italy*

We examine the properties of a recently proposed observationally viable alternative to homogeneous cosmology with smooth dark energy, the timescape cosmology. In the timescape model cosmic acceleration is realized as an apparent effect related to the calibration of clocks and rods of observers in bound systems relative to volume-average observers in an inhomogeneous geometry in ordinary general relativity. The model is based on an exact solution to a Buchert average of the Einstein equations with backreaction. The present paper examines a number of observational tests which will enable the timescape model to be distinguished from homogeneous cosmologies with a cosmological constant or other smooth dark energy, in current and future generations of dark energy experiments. Predictions are presented for: comoving distance measures;  $H(z)$ ; the equivalent of the dark energy equation of state,  $w(z)$ ; the  $Om(z)$  measure of Sahni, Shafieloo and Starobinsky; the Alcock–Paczyński test; the baryon acoustic oscillation measure,  $D_V$ ; the inhomogeneity test of Clarkson, Bassett and Lu; and the time drift of cosmological redshifts. Where possible, the predictions are compared to recent independent studies of similar measures in homogeneous cosmologies with dark energy. Three separate tests with indications of results in possible tension with the  $\Lambda$ CDM model are found to be consistent with the expectations of the timescape cosmology.

PACS numbers: 98.80.-k 98.80.Es 95.36.+x 98.80.Jk

## I. INTRODUCTION

The paradigm for our current standard model of the universe assumes that the universe is well-described by a geometry which is exactly homogeneous and isotropic, with additional Newtonian perturbations. The underlying geometry is assumed to be that of a Friedmann–Lemaître–Robertson–Walker (FLRW) geometry, and in matching the cosmological observables that derive from such a geometry, we have been led to the conclusion over the past decade that the present-day universe is dominated by a cosmological constant or other fluid-like “dark energy” with an equation of state,  $P = w\rho$ , which violates the strong energy condition.

Although the matter distribution was certainly very homogeneous at the epoch of last-scattering when the cosmic microwave background (CMB) radiation was laid down, however, in the intervening aeons the matter distribution has become very inhomogeneous through the growth of structure. Large scale surveys reveal the present epoch universe to possess a cosmic web of structure, dominated in volume by voids, with galaxy clusters strung in sheets and filaments that surround the voids, and thread them. Statistical homogeneity of this structure appears only to be reached by averaging on scales of order  $100h^{-1}$  Mpc or more, where  $h$  is the dimensionless parameter related to the Hubble constant by  $H_0 = 100h$  km sec<sup>-1</sup> Mpc<sup>-1</sup>. The problem of fitting a smooth geometry to a universe with such a lumpy mat-

ter distribution [1, 2] is a nontrivial one, but central to relating observations to the numerical values of the averaged parameters which describe the Universe and its evolution as a whole.

Given the observed inhomogeneity of the present epoch universe, a number of cosmologists have questioned whether the FLRW geometries are adequate as a description of the universe at late times [3]–[9]. In particular, the deduction that the universe is accelerating might in fact be a result of trying to fit the wrong cosmological model. One central question in the fitting problem is the issue of deriving the average evolution of the inhomogeneous geometry. If one considers irrotational dust cosmologies, and averages just inhomogeneous scalar quantities, in Buchert’s scheme [3] one finds an average of the Einstein equation in which there is a Friedmann-like evolution modified by backreaction [10, 11, 12],

$$\frac{3\dot{\bar{a}}^2}{\bar{a}^2} = 8\pi G\langle\rho\rangle - \frac{1}{2}\langle\mathcal{R}\rangle - \frac{1}{2}\mathcal{Q}, \quad (1)$$

$$\frac{3\ddot{\bar{a}}}{\bar{a}} = -4\pi G\langle\rho\rangle + \mathcal{Q}, \quad (2)$$

$$\partial_t\langle\rho\rangle + 3\frac{\dot{\bar{a}}}{\bar{a}}\langle\rho\rangle = 0, \quad (3)$$

$$\partial_t(\bar{a}^6\mathcal{Q}) + \bar{a}^4\partial_t(\bar{a}^2\langle\mathcal{R}\rangle) = 0, \quad (4)$$

where an overdot denotes a time derivative for observers comoving with the dust of density  $\rho$ ,  $\bar{a}(t) \equiv [\mathcal{V}(t)/\mathcal{V}(t_0)]^{1/3}$  with  $\mathcal{V}(t) \equiv \int_{\mathcal{D}} d^3x \sqrt{\det^3 g}$ , angle brackets denote the spatial volume average of a quantity, so that  $\langle\mathcal{R}\rangle \equiv \left(\int_{\mathcal{D}} d^3x \sqrt{\det^3 g} \mathcal{R}(t, \mathbf{x})\right) / \mathcal{V}(t)$  is the average spatial curvature, and

$$\mathcal{Q} = \frac{2}{3}(\langle\theta^2\rangle - \langle\theta\rangle^2) - 2\langle\sigma^2\rangle, \quad (5)$$

<sup>†</sup>Permanent address

\*Electronic address: David.Wiltshire@canterbury.ac.nz

is the kinematic backreaction,  $\sigma^2 = \frac{1}{2}\sigma_{\alpha\beta}\sigma^{\alpha\beta}$  being the scalar shear. We use units in which  $c = 1$ . Eq. (4) is an integrability condition needed to ensure that eq. (1) is the integral of eq. (2).

One must be careful in interpreting equations (1)–(5) since the spatial averages refer to average quantities which depend on the domain of integration on a spatial hypersurface. Observers measure invariants of the local metric, not a spatially averaged metric, and cosmological information comes to us on null geodesics. Given these problems, the Buchert approach has been criticised [13], and the whole area of backreaction is the subject of some debate and controversy. In recent work [14, 15, 16] I have developed an interpretation of solutions to the Buchert equations which circumvents the criticisms of Sec. 3 of ref. [13]. It differs from other approaches to the Buchert equations that have been used in the literature [17]–[22]. As well as circumventing objections that have been raised against Buchert averaging, the new interpretation has a conceptual basis which can be understood as an extension of the equivalence principle [23], and it leads to a quantitative model universe with predictions [14, 24] which thus far are in good agreement with observation. In particular, by Bayesian comparison the Riess07 gold supernovae Ia (SneIa) data set [25] agrees with the model predictions at a level which is statistically indistinguishable from the standard spatially flat  $\Lambda$ CDM [24, 26]. The same best-fit parameters also fit the angular scale of the sound horizon seen in CMB data, and the effective comoving baryon acoustic oscillation (BAO) scale seen in angular diameter tests of galaxy clustering statistics [14, 24].

Given these promising indications, it is important that the cosmology of refs. [14, 15] is developed well beyond the stage of what might be regarded as a “toy model”, so that it can be confronted by all the same observational tests that are applied to the  $\Lambda$ CDM model. For example, many current precision tests involve the detailed analysis of the CMB [28], and of galaxy clustering statistics [29]–[36]. To construct tests of similar precision will require the development of new numerical codes for the analysis of large datasets adapted to the present cosmology, analogous to those based on the decades of detailed work that have been applied to the standard cosmology.

Such goals represent an arduous project, and here I will simply take a few steps in the direction of confronting the observations. The aim of the present paper is not to present a detailed analysis of current data sets, but to outline a number of observable quantities which might be tested in future. Since the predictions obtained for a number of these quantities can be readily compared to existing independent analyses of homogeneous cosmologies with dark energy, I will make relevant comparisons where possible. I will confine the discussion here to average quantities which are relevant at all redshifts on scales greater than the scale of statistical homogeneity. Other relatively local tests which deal with quantities within the  $100h^{-1}$  Mpc scale of statistical homogeneity [14, 27] will be left to future work.

The plan of the papers is as follows. In Sec. II I will summarize the key features of the model introduced in refs. [14, 15], while also providing some further discussion. Additional technical details which were not provided in ref. [15] on account of space restrictions are given in the Appendices. In Sec. III I discuss the luminosity distance and angular diameter distance relations, and their interpretation in terms of the equivalent of a “dark energy equation of state”, which enables a direct comparison to recent studies to be made. In Sec. IV related diagnostics,  $H(z)$  and the  $Om(z)$  measure are evaluated and discussed in relation to recent studies. The Alcock–Paczyński and BAO tests are treated similarly in Sec. V. The expected nontrivial signature of a test of the Friedmann equation of Clarkson, Bassett and Lu is determined in Sec. VI. A prediction for the Sandage–Loeb test of the time drift of cosmological redshifts is presented in Sec. VII. Sec. VIII contains a concluding discussion.

## II. OVERVIEW OF THE TIMESCAPE MODEL

### A. Voids and walls

I will begin by briefly reviewing the two-scale “fractal bubble model” [14] which I am hereby renaming the “timescape model” [37], concentrating on the operational interpretation of observations. The model is constructed by identifying the observed scales most relevant to the observed present epoch inhomogeneous structure as being negatively curved *voids* and spatially flat *walls*, which surround bound structures.

Since galaxies and galaxy clusters formed from perturbations which were greater than critical density, then given an observable universe which on average has negative Ricci scalar curvature, we have a natural separation between walls and voids. As there is assumed to be a gradient in spatial curvature, it is assumed we can always enclose the bound structures which formed from overcritical perturbations within regions which are spatially flat on average, and marginally expanding at the boundary. These boundaries are called *finite infinity* regions [14], with local average metric

$$ds_{fi}^2 = -d\tau_w^2 + a_w^2(\tau_w) [d\eta_w^2 + \eta_w^2 d\Omega^2] . \quad (6)$$

The walls constitute the union of such finite infinity regions. Observationally they would correspond to all extended structures that contain galaxy clusters, namely sheets, filaments and knots [38].

Voids of a characteristic diameter  $30h^{-1}$  Mpc are observed to fill 40–50% of the universe at the present epoch [39]. In addition there are numerous minivoids, which have been well-studied in the local volume [40]. Together voids of all sizes appear to dominate the volume of the present epoch universe, the exact volume fraction depending on the empirical definition of a void in terms of some particular negative density contrast. In the two-scale approximation of refs. [14, 15] both the dominant

voids and minivoids are assumed to be characterized by the same negatively spatial curvature scale, with a metric at the void centres being given by

$$ds_{\mathcal{D}_v}^2 = -d\tau_v^2 + a_v^2(\tau_v) [d\eta_v^2 + \sinh^2(\eta_v)d\Omega^2] \quad (7)$$

We construct an average over the disjoint union of wall and void regions over the entire present horizon volume  $\mathcal{V} = \mathcal{V}_i \bar{a}^3$ , where

$$\bar{a}^3 = f_{vi} a_v^3 + f_{wi} a_w^3, \quad (8)$$

$f_{vi}$  and  $f_{wi} = 1 - f_{vi}$  being the respective initial void and wall volume fractions at last scattering. The finite infinity scale only becomes operationally defined once regions start collapsing and structure forms. Thus at last scattering a different interpretation of the wall and void components in (8) is required. At this epoch the wall fraction  $f_w$  is understood as that fraction of the present horizon volume which comprises perturbations whose combined mean density is the same as the mean density of the statistical ensemble of perturbations, including those beyond the horizon. The void fraction,  $f_v$ , is understood to be that (small) fraction of the present horizon volume in underdense perturbations which was not compensated by overdense perturbations at last scattering. It is convenient to rewrite (8) as  $f_v(t) + f_w(t) = 1$ , where  $f_w(t) = f_{wi} a_w^3 / \bar{a}^3$  is the *wall volume fraction* and  $f_v(t) = f_{vi} a_v^3 / \bar{a}^3$  is the *void volume fraction*.

## B. The scale of “statistical homogeneity”

In order to physically identify observables we must specify what is to be identified as a “particle” of dust. The question of what constitutes a particle of dust is not directly addressed in Buchert’s scheme, although perhaps implicitly many researchers think of galaxies as being the particles of dust, as historically this is the way the matter is treated in the FLRW model. However, galaxies evolve considerably over time and are not homogeneously distributed at the present epoch. Thus if we wish to follow cosmic evolution from the epoch of last scattering to the present, with no assumptions about homogeneity, then we must coarse grain the dust on scales over which mass flows can be neglected, so that each dust particle remains of a roughly fixed mass, even if the mass differs somewhat from particle to particle.

Here we take a “dust particle” to be of at least the scale of statistical homogeneity,  $100h^{-1}$  Mpc or somewhat larger [41]. The *scale of statistical homogeneity* is taken to refer to a scale volume within which the structure of voids and walls is roughly similar, if such a box is chosen at random on a spatial slice in the observable universe at late epochs. It is important to realise such volumes will *not* have the same density. Rather they will have a density which is distributed about a mean with a standard deviation of order several percent, by an argument that follows from eq. (9) below.

We must stress that the universe is not considered to be a FLRW model, and our terminology of a “scale of statistical homogeneity” is not the same as in a FLRW model. A scale of homogeneity, in its sense in the FLRW model, is not assumed to exist. The principal difference is that in a FLRW model the density of the observable universe, sampled over the present horizon volume, is assumed to be the mean density of the ensemble from which our observable horizon volume was drawn. In the FLRW case the standard deviation of the density of spatial volumes would decrease to zero as one sampled ever larger volumes greater than the homogeneity scale, as is the case for any stationary stochastic process [43].

Such a state of affairs cannot be expected to prevail, however, given cosmic variance and an initial spectrum of density contrasts of all possible length scales which are nested within each other, which is the expectation from primordial inflation. Given cosmic variance, then as one samples larger and larger volumes that become comparable with the horizon volume, one is dealing with fewer and fewer individual fluctuations rather than a statistical ensemble. The assumption in the timescape scenario is that the present horizon volume is underdense relative to the ensemble mean density, which at last-scattering is extremely close to critical.

The fact that it does nonetheless make sense to think of a “scale of statistical homogeneity” as above, however, is a simple consequence of the fact that although the density perturbations have all possible length scales, the magnitude of these contrasts was severely bounded at the time of last scattering. In other words, given a universe which was close to homogeneous at last scattering, it can only evolve so far from homogeneity within the finite age of the universe.

The relevant scale for a cutoff to the “scale of statistical homogeneity” is scale of the largest acoustic wave in the plasma at last scattering – of order  $110h^{-1}$  Mpc. The simple reason for such a cutoff, is that below this scale initial density contrasts may be amplified by acoustic waves in the plasma, so that rather than having initial density contrasts of say  $\delta\rho/\rho \sim 10^{-4}$  in nonbaryonic dark matter, the initial density contrasts will be somewhat larger. The second acoustic peak in the CMB anisotropy spectrum – i.e., the first refraction peak – for example, will amplify the density contrast of underdense regions, and may therefore be the feature of the primordial spectrum responsible for the fact that the dominant void fraction is associated to a specific scale  $30h^{-1}$  Mpc [39].

Given that some initial density perturbations are amplified below the acoustic scale, and that the CMB anisotropy spectrum is fairly flat at long wavelengths, the acoustic scale provides a cutoff analogous the cutoff between the nonlinear and linear regimes of structure formation, although here there is no single global FLRW model about which such regimes linear are defined [42]. Below the scale of statistical homogeneity we will typically find density contrasts  $|\delta\rho/\rho| \sim 1$  which characterize the nonlinear regime, as is the observed case for

$30h^{-1}$  Mpc diameter voids [39]. Above the acoustic scale, we can be sure that the perturbations at last scattering have very similar amplitudes as a function of scale. Although the perturbations in the photon–baryon plasma have contrasts  $\delta\rho/\rho \sim 10^{-5}$  at this epoch, the density contrast in nonbaryonic dark matter is expected to be somewhat larger; e.g., of order  $\delta\rho/\rho \sim 10^{-4}$ – $10^{-3}$ , depending on one’s dark matter model.

The standard deviation of the density of cells on scales larger than the scale of statistical homogeneity can be estimated crudely by assuming that such cells each evolve as an independent Friedmann universe from a smooth perturbation at the epoch of last scattering. This approximation is justified since the relevant scale is the one over which there are no appreciable average mass flows from one dust cell to another. We assume that the backreaction contributions do not dominate the volume–average evolution, and make our rough estimate from the Friedmann equation with pressureless dust only, for which

$$a_0^2 H_0^2 (\Omega_{M0} - 1) = a^2(t) H^2(t) [\Omega_M(t) - 1]$$

This leads to a present epoch density contrast

$$\delta\rho_0 \simeq \left(\frac{H}{H_0}\right)^2 \frac{\delta\rho_t}{(1+z)^2}, \quad (9)$$

where the density contrast is relative to the critical density, so that  $\delta\rho_t = \Omega_M(t) - 1$  etc, where  $\Omega_M$  is a density parameter for the isolated region only. (Physically, the critical density is that within a spatially flat wall region.) Thus if we take  $\delta\rho_t \simeq 10^{-4}$  at last scattering, when  $z \simeq 1090$  and when  $H \simeq 2/(3t)$  with  $t \simeq 380,000$  yr, we are led to  $\delta\rho_0 \simeq 0.025/h^2 \simeq 0.06$  if  $h \simeq 0.65$ .

This crude estimate can be compared to the actual density variance determined from large scale structure surveys [44, 45]. Sylos Labini *et al* [45] have recently determined the variance in the number density of luminous red galaxies (LRGs) in the SDSS-DR7 by dividing the full sample of 53,066 galaxies in the redshift range  $10^{-4} < z < 0.3$  into  $N$  equal nonoverlapping volumes. Over the range  $4 \leq N \leq 15$ , the standard deviation is found to be of order 8%, consistent with an earlier measurement of 7% by Hogg *et al* [44] in a smaller LRG sample. These values are very close to our order of magnitude estimate of 6%. Provided LRGs are correlated to the actual density, then the variance in the percentage density contrast will be commensurate. In fact, such variances can be used to constrain the dark matter density contrast at last scattering. A measurement of 8% would indicate, reversing the argument above, that a contrast of  $\delta\rho/\rho \sim 10^{-3}$  in nonbaryonic dark matter at last scattering is an order of magnitude too large.

Given a nearly scale–invariant spectrum of density perturbations, with perturbations nested in perturbations, our expectation is that the variance in density should not decrease appreciably if sample volumes are increased at nearby redshifts. In principle, it should be possible to calculate it as a function of scale, given the constraints

from the CMB anisotropy spectrum at long wavelengths. For spatial slices at higher redshifts, looking further back in time, the variance would decrease in accord with (9) – provided that a sample of objects such as LRGs can be found which does not exhibit strong evolutionary effects over the range of redshifts in question.

Of course, the estimate based on (9) could be further refined to take backreaction into account; but further accuracy can only be gained when one has a tighter estimate of the dark matter density contrast than simply an order of magnitude. Furthermore, the statistical physics of cosmic structures in the timescape scenario may well differ from that of the FLRW model [43] in significant ways; one has to revisit the whole problem from first principles.

In summary, the observed universe is not assumed to be homogeneous or to approach any single global FLRW model at any scale. The “statistical homogeneity scale” – which will coincide roughly with the BAO scale – represents a scale above which the variance in density contrasts is bounded at the 10% level, and below which density contrasts become as large as they can possibly be.

### C. The bare Hubble flow and bare cosmological parameters

Given our identification of dust particles coarse-grained at the scale of statistical homogeneity, and possible very large differences in spatial curvature and gravitational energy within such a cell, we do not assume that Buchert average time parameter,  $t$ , is the relevant parameter measured by every isotropic observer – those who see an isotropic CMB – within any dust cell. Rather it is the time parameter measured by an isotropic observer whose local spatial curvature happens to coincide with the Buchert volume–average spatial curvature  $\langle \mathcal{R} \rangle$ . We employ an ansatz of an underlying quasilocal uniform Hubble flow within a dust cell, below the scale of statistical homogeneity, in terms of local proper lengths with respect to local proper times, which both vary with gradients in spatial curvature and gravitational energy. This ansatz provides an implicit resolution of the Sandage–de Vaucouleurs paradox [14], and can be understood in terms of a generalization of the equivalence principle [23].

The metrics (6) and (7) are assumed to represent the local geometry for isotropic observers at finite infinity and at void centres respectively. Within the scale of statistical homogeneity the metrics (6) and (7) are assumed to be patched together with a condition of uniform quasilocal bare Hubble flow [14, 23]

$$\bar{H} = \frac{da_w}{d\tau_w} = \frac{da_v}{d\tau_v}, \quad (10)$$

which will preserve isotropy of the CMB. The mean CMB temperature and angular anisotropy scale will vary with the gradients in gravitational energy and spatial curvature, however.

For the purpose of the Buchert average we refer all quantities to one set of volume–average clocks: those that keep the time parameter  $t$  of eqs. (1)–(5) so that

$$\bar{H} \equiv \frac{\dot{\bar{a}}}{\bar{a}} = \bar{\gamma}_w H_w = \bar{\gamma}_v H_v \quad (11)$$

where

$$H_w \equiv \frac{1}{a_w} \frac{da_w}{dt}, \quad \text{and} \quad H_v \equiv \frac{1}{a_v} \frac{da_v}{dt}, \quad (12)$$

and

$$\bar{\gamma}_w \equiv \frac{dt}{d\tau_w}, \quad \text{and} \quad \bar{\gamma}_v \equiv \frac{dt}{d\tau_v}, \quad (13)$$

are lapse functions of volume–average time,  $t$ , relative to wall and void–centre observers respectively. The ratio of the relative Hubble rates  $h_r = H_w/H_v < 1$  is related to the wall lapse function by

$$\bar{\gamma}_w = 1 + \frac{(1 - h_r)f_v}{h_r}, \quad (14)$$

and  $\bar{\gamma}_v = h_r \bar{\gamma}_w$ .

The Buchert equations for pressureless dust with volume–average density  $\bar{\rho}_M$  are solved [15] in the two–scale approximation by assuming that there is no backreaction within walls and voids separately [46], but only in the combined average. With this assumption, the kinematic backreaction term becomes [14]

$$\mathcal{Q} = 6f_v(1 - f_v)(H_v - H_w)^2 = \frac{2\dot{f}_v^2}{3f_v(1 - f_v)}. \quad (15)$$

The resulting independent Buchert equations consist of two coupled nonlinear ordinary differential equations [14] for  $\bar{a}(t)$  and  $f_v(t)$ , which may be written as

$$\bar{\Omega}_M + \bar{\Omega}_k + \bar{\Omega}_\mathcal{Q} = 1, \quad (16)$$

$$\bar{a}^{-6} \partial_t (\bar{\Omega}_\mathcal{Q} \bar{H}^2 \bar{a}^6) + \bar{a}^{-2} \partial_t (\bar{\Omega}_k \bar{H}^2 \bar{a}^2) = 0, \quad (17)$$

where

$$\bar{\Omega}_M = \frac{8\pi G \bar{\rho}_{M0} \bar{a}_0^3}{3\bar{H}^2 \bar{a}^3}, \quad (18)$$

$$\bar{\Omega}_k = \frac{-k_v f_{vi}^{2/3} f_v^{1/3}}{\bar{a}^2 \bar{H}^2}, \quad (19)$$

$$\bar{\Omega}_\mathcal{Q} = \frac{-\dot{f}_v^2}{9f_v(1 - f_v)\bar{H}^2}, \quad (20)$$

are the volume–average or “bare” matter density, curvature density and kinematic backreaction density parameters respectively,  $\bar{a}_0$  and  $\bar{\rho}_{M0}$  being the present epoch values of  $\bar{a}$  and  $\bar{\rho}_M$ . The average curvature is due to the voids only, which are assumed to have  $k_v < 0$ . The volume–average deceleration parameter is given by

$$\bar{q} \equiv \frac{-\ddot{\bar{a}}}{\bar{H}^2 \bar{a}} = \frac{1}{2} \bar{\Omega}_M + 2\bar{\Omega}_\mathcal{Q} \quad (21)$$

Equations (16), (17) are readily integrated to yield an exact solution [15], which is listed in Appendix A, together with its simple tracking limit in Appendix B. For initial conditions at last scattering consistent with observations, solutions are found to reach within 1% of the tracking limit by a redshift  $z \sim 37$  [15]. Thus the tracker solution will be used for the purposes of the specific cosmological tests which are investigated in this paper [47].

It should be noted that for the solution found in ref. [15], the backreaction term is at most of order 4.2% [48]. Its redshift dependence for the best–fit parameters is exhibited in Fig. 1. Although  $\bar{\Omega}_\mathcal{Q}$  is negative, it is never large enough relative to  $\bar{\Omega}_M$  to dominate the r.h.s. of (21) and give volume average cosmic acceleration. The backreaction itself is not the sole reason for apparent cosmic acceleration; that is also a question of how volume–average evolution is interpreted in terms of a local metric.

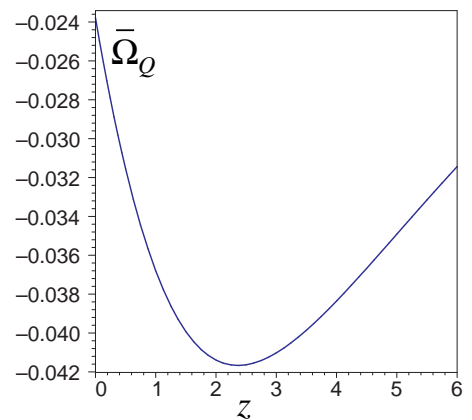


FIG. 1: The bare backreaction density parameter  $\bar{\Omega}_\mathcal{Q}$  as a function of redshift for the timescape model with  $f_{v0} = 0.762$ ,  $H_0 = 61.7 \text{ km sec}^{-1} \text{ Mpc}^{-1}$ .

#### D. Dressed cosmological parameters

One must take care in physically interpreting the solution of the Buchert equation, since it does not represent a single exact solution of Einstein’s equations, but rather a spatial average. Observers measure invariants of the local metric, and information carried by radial null geodesics from distant parts of the universe. In ref. [14] a means of interpreting the Buchert equation was developed as follows.

First, since cosmological information is obtained by a radial spherically symmetric average, we construct a spherically symmetric geometry relative to an observer who measures volume–average time, and with a spatial volume scaling as  $\bar{a}^3(t)$ ,

$$d\bar{s}^2 = -dt^2 + \bar{a}^2(t) d\bar{\eta}^2 + \mathcal{A}(\bar{\eta}, t) d\Omega^2, \quad (22)$$

where the area quantity,  $\mathcal{A}(\bar{\eta}, t)$ , satisfies  $\int_0^{\bar{\eta}} d\bar{\eta} \mathcal{A}(\bar{\eta}, t) = \bar{a}^2(t) \mathcal{V}_i(\bar{\eta}_{\mathcal{H}})/(4\pi)$ ,  $\bar{\eta}_{\mathcal{H}}$  being the conformal distance to the particle horizon relative to an observer at  $\bar{\eta} = 0$ , since we have chosen the particle horizon as the scale of averaging. The metric (22) is spherically symmetric by construction, but is not a Lemaître–Tolman–Bondi (LTB) solution since it is not an exact solution of Einstein’s equations, but rather of the Buchert average of the Einstein equations.

In terms of the wall time,  $\tau_w$ , of finite infinity observers the metric (22) is

$$d\bar{s}^2 = -\bar{\gamma}_w^2(\tau_w) d\tau_w^2 + \bar{a}^2(\tau_w) d\bar{\eta}^2 + \mathcal{A}(\bar{\eta}, \tau_w) d\Omega^2. \quad (23)$$

However, this geometry, which has negative spatial curvature is not the locally measured geometry at finite infinity, which is given instead by (6). Since (6) is not a global geometry, we match (6) to (23) to obtain a dressed wall geometry, which is effectively the closest thing there is to a FLRW geometry adapted to the rods and clocks of wall observers. The matching is achieved in two steps. First we conformally match radial null geodesics of (6) and (23), bearing in mind that null geodesics are unaffected by an overall conformal scaling. This leads to a relation

$$d\eta_w = \frac{f_{wi}^{1/3} d\bar{\eta}}{\bar{\gamma}_w (1 - f_v)^{1/3}} \quad (24)$$

along the geodesics. Second, we account for volume and area factors by taking  $\eta_w$  in (6) to be given by the integral of (24).

The wall geometry (6), which may also be written

$$ds_{fi}^2 = -d\tau_w^2 + \frac{(1 - f_v)^{2/3} \bar{a}^2}{f_{wi}^{2/3}} [d\eta_w^2 + \eta_w^2 d\Omega^2], \quad (25)$$

on account of (8), is a local geometry only valid in spatially flat wall regions. We now use (24) and its integral to extend this metric beyond the wall regions to obtain the dressed global metric

$$\begin{aligned} ds^2 &= -d\tau_w^2 + \frac{\bar{a}^2}{\bar{\gamma}_w^2} d\bar{\eta}^2 + \frac{\bar{a}^2 (1 - f_v)^{2/3}}{f_{wi}^{2/3}} \eta_w^2(\bar{\eta}, \tau_w) d\Omega^2 \\ &= -d\tau_w^2 + \bar{a}^2(\tau_w) [d\bar{\eta}^2 + r_w^2(\bar{\eta}, \tau_w) d\Omega^2] \end{aligned} \quad (26)$$

where  $a \equiv \bar{\gamma}_w^{-1} \bar{a}$ , and

$$r_w \equiv \bar{\gamma}_w (1 - f_v)^{1/3} f_{wi}^{-1/3} \eta_w(\bar{\eta}, \tau_w).$$

Whereas (6) represents a local geometry only valid in spatially flat wall regions, the dressed geometry (26) extends as an average effective geometry [49] to the cosmological scales parameterized by the volume–average conformal time, which satisfies  $d\bar{\eta} = dt/\bar{a} = d\tau_w/a$ . Since the geometry on cosmological scales does not have constant Gaussian curvature the average metric (26), like (22), is spherically symmetric but not homogeneous.

In trying to fit a FLRW model to the universe, the cosmological parameters we obtain effectively have numerical values close to those of the dressed geometry (26). In particular, we infer a dressed matter density parameter

$$\Omega_M = \bar{\gamma}_w^3 \bar{\Omega}_M, \quad (27)$$

a dressed Hubble parameter

$$H \equiv \frac{1}{a} \frac{da}{d\tau} = \frac{1}{\bar{a}} \frac{d\bar{a}}{d\tau_w} - \frac{1}{\bar{\gamma}_w} \frac{d\bar{\gamma}_w}{d\tau_w} = \bar{\gamma}_w \bar{H} - \dot{\bar{\gamma}}_w, \quad (28)$$

and similarly a dressed deceleration parameter, where the overdot still denotes a derivative with respect to volume–average time. As demonstrated in refs. [14, 15] in a void–dominated universe the dressed deceleration parameter is negative at late epochs, even though the bare deceleration parameter (21) is positive. Thus cosmic acceleration is realised as an apparent effect due to the variance of local geometry from the average, leading to variance in the calibration of clocks and rods.

In the rest of the paper we will drop the subscript “w” from both  $\tau_w$  and  $\bar{\gamma}_w$ , as we will not need to make explicit reference to the time measured in void centres. Thus  $\tau$  and  $\bar{\gamma}$  will be assumed to refer to wall time.

### III. COMOVING DISTANCE $D(z)$ AND EQUIVALENT OF THE “EQUATION OF STATE”

In testing fluid–like dark energy scenarios, or modified gravity theories that can be cast as an effective fluid with an equation of state  $P = w\rho$ , a common question is: how can the equation of state parameter,  $w(z)$ , be constrained as a function of redshift? Unfortunately, if dark energy is some purely unknown physics, then it is completely unclear how one should expand it as a power series. A linear series in  $z$  will not converge for  $z > 1$ , for example, so series in  $z/(1+z)$  are sometimes considered. Unless one has a precise physical model of dark energy to be tested, then any constraints are completely dependent on how one chooses to characterize such a power series. When constraints on the value of  $w$  from cosmological observations are quoted in the literature, it is often on the basis that  $w$  is simply a constant, even though there is no known physics for making such an assumption, apart from the cosmological constant case of  $w = -1$ .

In this section I will derive the equivalent of the “equation of state” style observational tests, although the terminology “equation of state” does not have a meaning in terms of actual observables, given that the model in question is not characterized by a fluid with  $P_D = w\rho_D$ . Let us recall that in the case of the standard FLRW models, the equation of continuity for such a dark energy component in a background universe with scale factor  $a(t)$ , viz.,

$$\dot{\rho}_D + 3\frac{\dot{a}}{a}(1+w)\rho_D = 0, \quad (29)$$

may be integrated to give

$$\ln\left(\frac{\rho_D}{\rho_{D0}}\right) = \int \frac{3[1+w(z)]dz}{1+z} \quad (30)$$

using  $a_0/a = 1+z$ , where it is assumed that the equation of state parameter varies with redshift. To obtain an expression for the luminosity distance one substitutes

$$r_{\text{FLRW}} \equiv \int_t^{t_0} \frac{dt}{a} = \int_a^{a_0} \frac{da}{a\dot{a}} = \int_0^z \frac{dz'}{a_0 H_0 \sqrt{\Omega_{M0}(1+z')^3 + \Omega_{D0} \exp\left[3 \int_0^{z'} \frac{(1+w(z''))dz''}{1+z''}\right]}}, \quad (32)$$

where  $\Omega_{M0} = 8\pi G\rho_{M0}/(3H_0^2)$  and  $\Omega_{D0} = 8\pi G\rho_{D0}/(3H_0^2) = 1 - \Omega_{M0}$ . The standard luminosity distance is then given by  $d_L = a_0 r_{\text{FLRW}}(1+z)$ . The quantity

$$D = a_0 r_{\text{FLRW}} = \frac{d_L}{1+z} \quad (33)$$

is the comoving distance quantity directly related to the luminosity distance. The angular diameter distance is also related by

$$d_A = \frac{D}{1+z} = \frac{d_L}{(1+z)^2}. \quad (34)$$

We observe from (32) that  $H_0 D$  does not depend on the value of the Hubble constant,  $H_0$ , but only directly on  $\Omega_{M0}$ .

Given observed quantities such as the apparent luminosity–redshift relation or an angular size–redshift relation for standard candles or standard rulers, we can take derivatives of (32) to obtain

$$w(z) = \frac{\frac{2}{3}(1+z)D'^{-1}D'' + 1}{\Omega_{M0}(1+z)^3 H_0^2 D'^2 - 1} \quad (35)$$

where prime denotes a derivative with respect to  $z$ . This gives a formal equation of state to any comoving distance relation, assuming an underlying spatially flat dark energy model. Such a relation can be applied to observed distance measurements, regardless of whether the underlying cosmology has dark energy or not. We should note, however, that such a  $w(z)$  has first and second derivatives of the observed quantities, and so is much more difficult to determine observationally than direct fits to a quantity such as  $D(z)$ .

For the timescape universe, equivalent comoving, angular diameter and luminosity distances can be defined in terms of the dressed geometry (6). We have a dressed luminosity distance relation

$$d_L = a_0(1+z)r_w, \quad (36)$$

(30) in the spatially flat Friedmann equation for matter plus dark energy,

$$\frac{\dot{a}^2}{a^2} = \frac{8\pi G}{3} \left[ \rho_{M0} \left(\frac{a_0}{a}\right)^3 + \rho_D \right] \quad (31)$$

and uses the resulting expression for  $\dot{a}$ , to determine the conformal time integral

where  $a_0 = \bar{\gamma}_0^{-1}\bar{a}_0$ , and the *effective comoving distance* to a redshift  $z$  is  $D = a_0 r_w$ , where

$$r_w = \bar{\gamma}(1-f_v)^{1/3} \int_t^{t_0} \frac{dt'}{\bar{\gamma}(t')(1-f_v(t'))^{1/3}\bar{a}(t')}. \quad (37)$$

As discussed in Sec. II, since spatial sections are not of constant Gaussian curvature this effective comoving distance represents a fit to our spatially flat rods once radial null geodesics are conformally matched, and geometric factors are taken into account.

For the tracker solution (B1), (B2) the cosmological redshift satisfies

$$z+1 = \frac{\bar{a}_0\bar{\gamma}}{\bar{a}\bar{\gamma}_0} = \frac{(2+f_v)f_v^{1/3}}{3f_{v0}^{1/3}\bar{H}_0 t} = \frac{2^{4/3}t^{1/3}(t+b)}{f_{v0}^{1/3}\bar{H}_0 t(2t+3b)^{4/3}}, \quad (38)$$

where

$$b = \frac{2(1-f_{v0})(2+f_{v0})}{9f_{v0}\bar{H}_0}. \quad (39)$$

The integral in (37) is readily evaluated to give

$$\begin{aligned} d_A &= \frac{D}{1+z} = (t)^{\frac{2}{3}} \int_t^{t_0} \frac{2 dt'}{(2+f_v(t'))(t')^{2/3}} \\ &= t^{2/3}(\mathcal{F}(t_0) - \mathcal{F}(t)) \end{aligned} \quad (40)$$

where

$$\begin{aligned} \mathcal{F}(t) &= 2t^{1/3} + \frac{b^{1/3}}{6} \ln\left(\frac{(t^{1/3}+b^{1/3})^2}{t^{2/3}-b^{1/3}t^{1/3}+b^{2/3}}\right) \\ &\quad + \frac{b^{1/3}}{\sqrt{3}} \tan^{-1}\left(\frac{2t^{1/3}-b^{1/3}}{\sqrt{3}b^{1/3}}\right). \end{aligned} \quad (41)$$

It is straightforward now to compare distance measurements in the timescape model with those in spatially flat  $\Lambda$ CDM models. The timescape model which best-fits the Riess07 gold data set had a void fraction  $f_{v0} = 0.76_{-0.09}^{+0.12}$ , and dressed Hubble constant  $H_0 =$

$61.7^{+1.2}_{-1.1} \text{ km sec}^{-1} \text{ Mpc}^{-1}$ , where  $1\sigma$  uncertainties are quoted [24]. In Fig. 2 we plot

$$H_0 D = H_0 t^{2/3} [\mathcal{F}(t_0) - \mathcal{F}(t)](1+z) \quad (42)$$

for the best-fit model with  $f_{v0} = 0.762$ , as compared to three spatially flat  $\Lambda$ CDM models with different values of  $\Omega_{M0}$ , (or of  $\Omega_{\Lambda0} = 1 - \Omega_{M0}$ ). Fig. 2 shows that over redshifts between the present epoch and last scattering, the timescape model interpolates between  $\Lambda$ CDM models with different values of  $\Omega_{M0}$ . For redshifts  $z \lesssim 1.5$   $D_{\text{TS}}$  is very close to  $D_{\Lambda\text{CDM}}$  for the parameter values  $(\Omega_{M0}, \Omega_{\Lambda0}) = (0.34, 0.66)$  (model (ii)) which best-fit the Riess07 SNeIa data only [24]. For very large redshifts that approach the surface of last scattering,  $z \lesssim 1100$ , on the other hand,  $D_{\text{TS}}$  very closely matches  $D_{\Lambda\text{CDM}}$  for the parameter values  $(\Omega_{M0}, \Omega_{\Lambda0}) = (0.249, 0.751)$  (model (i)) which best-fit WMAP5 only [28]. Over redshifts  $2 \lesssim z \lesssim 10$ , at which scales independent tests are conceivable,  $D_{\text{TS}}$  makes a transition over corresponding curves of  $D_{\Lambda\text{CDM}}$  with intermediate values of  $(\Omega_{M0}, \Omega_{\Lambda0})$ . The  $D_{\Lambda\text{CDM}}$  curve for joint best fit parameters to SNeIa, BAO measurements and WMAP5 [28],  $(\Omega_{M0}, \Omega_{\Lambda0}) = (0.279, 0.721)$  is best-matched over the range  $5 \lesssim z \lesssim 6$ , for example.

Given the difference of  $D_{\text{TS}}$  from any single  $D_{\Lambda\text{CDM}}$  curve becomes pronounced only in the range  $2 \lesssim z \lesssim 6$ , it may be difficult to distinguish the models on the basis of the measurement of  $d_A$  alone from BAO surveys, which

will be able to measure  $d_A(z)$  up to 1% to  $z < 3$ . However, joint measurements of other parameters, such as  $H(z)$ , may make for definitive tests, as will be discussed later. Gamma-ray bursters (GRBs) do probe distances to redshifts  $z \lesssim 8.3$ , and could be very useful. There has already been much work deriving Hubble diagrams using GRBs. (See, e.g., [50].) It would appear that more work needs to be done to nail down systematic uncertainties, but GRBs may provide a definitive test in future. An analysis of the timescape model Hubble diagram using 69 GRBs has just been performed by Schaefer [51], who finds that it fits the data better than the concordance  $\Lambda$ CDM model, but not yet by a huge margin. As more data is accumulated, it should become possible to distinguish the models.

### A. Effective “dark energy equation of state”

The equivalent of an “equation of state”,  $w(z)$ , for the timescape model may be determined from (35) and (40). The specific analytic expressions for the first and second derivatives of  $D$  are

$$\frac{dD}{dz} = \frac{t \left[ (2t - b) d_A + (2t + 3b)^2 \right]}{3(2t^2 + 3bt + 2b^2)}, \quad (43)$$

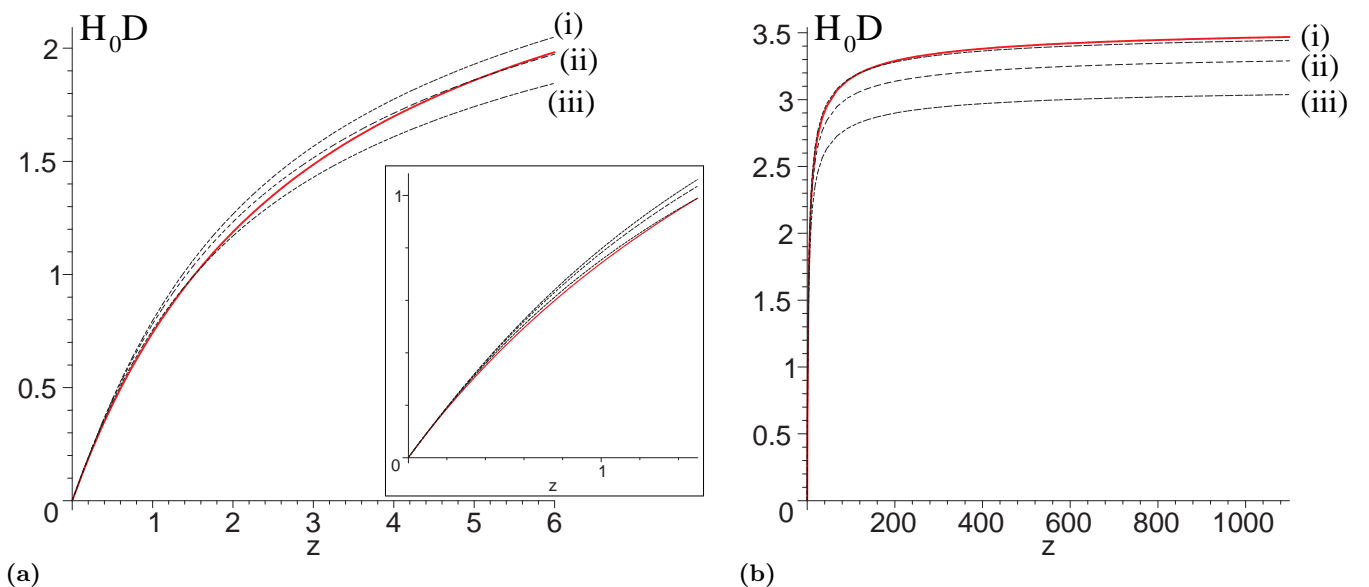


FIG. 2: The effective comoving distance  $H_0 D(z)$  is plotted for the best-fit timescape model, with  $f_{v0} = 0.762$ , (solid line, red online); and for various spatially flat  $\Lambda$ CDM models (dashed lines). The parameters for the dashed lines are (i)  $\Omega_{M0} = 0.249$  (best-fit to WMAP5 only); (ii)  $\Omega_{M0} = 0.279$  (joint best-fit to SNeIa, BAO and WMAP5); (iii)  $\Omega_{M0} = 0.34$  (best-fit to Riess07 SNeIa only). Panel (a) shows the redshift range  $z < 6$ , with an inset for  $z < 1.5$ , which is the range tested by current SNeIa data. Panel (b) shows the range  $z < 1100$  up to the surface of last scattering, tested by WMAP5.

$$\frac{d^2 D}{dz^2} = \frac{-t(2t+3b)[2(t+b)(2t+5b)(2t^2+3bt-b^2)d_A + (2t+3b)(8t^4+26bt^3+53b^2t^2+56b^3t+18b^4)]}{9(1+z)(2t^2+3bt+2b^2)^3} \quad (44)$$

In these expressions  $d_A$  is given by (40) and  $t$  is given implicitly in terms of the redshift,  $z$ , via (38). We now substitute (43) and (44) in (35) and use the fact that by (B9),  $H_0 = (4f_{v0}^2 + f_{v0} + 4)\bar{H}_0/[2(2 + f_{v0})]$ , to obtain

$$w = \frac{(40t^5 - 28bt^4 - 274b^2t^3 - 349b^3t^2 - 92b^4t + 24b^5)d_A + t(2t+3b)^2(20t^3 + 56bt^2 + 47b^2t - 4b^3)}{\left\{(2t-b)d_A + (2t+3b)^2\right\} \left\{A_0(z+1)^3t^2 \left[(2t-b)d_A + (2t+3b)^2\right]^2 - 9(2t^2+3bt+2b^2)^2\right\}} \quad (45)$$

where

$$A_0 = \frac{\Omega_{M0}(4f_{v0}^2 + f_{v0} + 4)^2}{4(2 + f_{v0})^2} \quad (46)$$

and  $d_A$  is given by (40)–(39). In fact,  $\Omega_{M0} = \frac{1}{2}(1 - f_{v0})(2 + f_{v0})$ , so that

$$A_0 = \frac{(1 - f_{v0})(4f_{v0}^2 + f_{v0} + 4)^2}{8(2 + f_{v0})}.$$

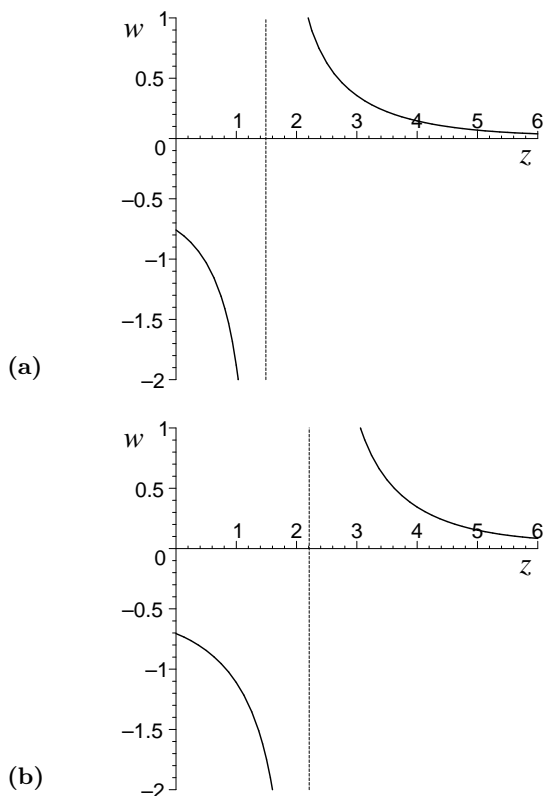


FIG. 3: The artificial equivalent of an equation of state (45), constructed using the effective comoving distance (35), plotted for the timescape tracker solution with best-fit value  $f_{v0} = 0.762$ , and two different values of  $\Omega_{M0}$ : (a) the canonical dressed value  $\Omega_{M0} = \frac{1}{2}(1 - f_{v0})(2 + f_{v0}) = 0.33$ ; (b)  $\Omega_{M0} = 0.279$ .

Since the  $w(z)$  expression is an artificial mathematical construction for the present model, we can also determine  $w(z)$  if a value of  $\Omega_{M0}$  different from the canonical  $\frac{1}{2}(1 - f_{v0})(2 + f_{v0})$  is assumed. In this way, we arrive at the example  $w(z)$  curves plotted in Fig. 3. The fact that the denominator of (45) goes through zero means that  $w(z)$  becomes formally infinite and changes sign at a value of  $z$  which depends on the value of  $\Omega_{M0}$  assumed [52]. This feature illustrates how pointless it is to talk about an equation of state of dark energy, or to choose to “reconstruct”  $w(z)$  if the underlying unknown physics has nothing to do with a fluid in the vacuum of space. What is actually measured is a quantity such as  $D(z)$ , illustrated in Fig. 2, and this is perfectly smooth.

Phenomenologically, for the canonical best-fit dressed value of  $\Omega_{M0} = 0.33$  [24], one finds that  $w(0) \simeq -0.758$  and that  $w(z)$  crosses the “phantom divide”  $w(z) = -1$  at  $z \simeq 0.464$ . The average value of  $w(z) \simeq -1$  on the range  $z \lesssim 0.7$ , while the average value of  $w(z) < -1$  if the range of redshifts is extended to higher values. This agrees with the evidence of the Snela data.

In fact, in a recent study [53] which examines constraints on the equation of state by combining the Constitution Snela data [56] with WMAP5 [28] and SDSS constraints, Zhao and Zhang find 95% evidence in favour of a model with  $w(z) > -1 \in (0.25, 0.5)$ ,  $w(z) < -1 \in (0.5, 0.75)$ , meaning that  $w(z)$  must cross the phantom divide in the range  $0.25 < w < 0.75$ . The fiducial model of Fig. 3(a) crosses the phantom divide almost in the centre of this redshift range.

Another recent investigation [54] draws different conclusions about evidence for dynamical dark energy. However, while the results of Serra *et al* [54] are consistent with a cosmological constant at the  $2\sigma$  level, they are also consistent with the best-fit timescape model at the same level, as illustrated in Fig. 4. The different conclusions drawn by the authors of refs. [53] and [54] result not only from using somewhat different data sets, but also from differences in the treatments of data bins.

In considering Fig. 4 it should also be borne in mind that there are significant systematic issues between the SALT and MLCS data reduction methods, as will be discussed in Sec. VIII. The Union [55] and Constitution [56] compilations use the SALT method. A new analysis of 103 SDSS-II Snela [57] in the redshift range,  $0.04 <$

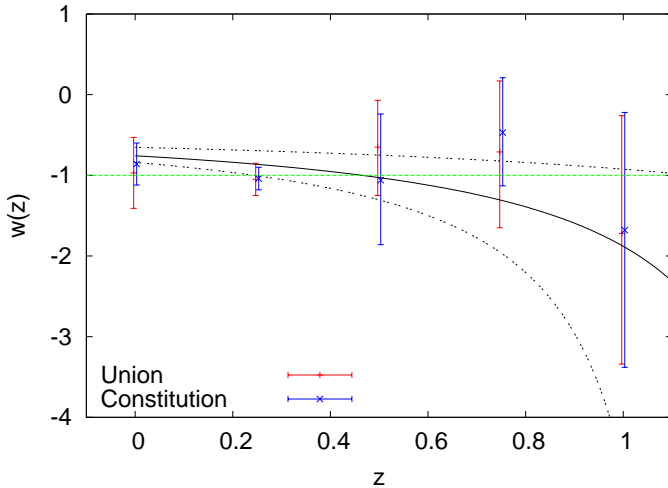


FIG. 4: The artificial equivalent of an equation of state (45) is compared with a recent analysis of Serra *et al* [54]. The third panel of Fig. 1 of ref. [54] is combined with the curve of  $w(z)$  for the best-fit value  $f_{v0} = 0.76^{+0.12}_{-0.09}$  (solid curve;  $1\sigma$  limits dotted curves). Following ref. [54]  $2\sigma$  uncertainties are plotted. The  $1\sigma$  uncertainties are tabulated in Table I.

redshift	$w_U$	$w_C$	$w_{TS}$
0.0	$-0.97 \pm 0.22$	$-0.86 \pm 0.13$	$-0.76^{+0.11}_{-0.07}$
0.25	$-1.05 \pm 0.10$	$-1.04 \pm 0.07$	$-0.86^{+0.17}_{-0.15}$
0.5	$-0.65^{+0.29}_{-0.30}$	$-1.06^{+0.41}_{-0.40}$	$-1.02 \pm 0.28$
0.75	$-0.71^{+0.44}_{-0.47}$	$-0.47^{+0.34}_{-0.33}$	$-1.31^{+0.49}_{-0.65}$
1.0	$-1.72^{+0.73}_{-0.81}$	$-1.68^{+0.73}_{-0.85}$	$-1.88^{+0.96}_{-2.76}$

TABLE I: Values of  $w(z)$  determined by Serra *et al* [54] using a standard FLRW cosmology are compared to the artificial equivalent of  $w(z)$  for the timescape model:  $w_U$  and  $w_C$  are the values determined by combining WMAP5 CMB and SDSS-DR7 BAO data with the Union and Constitution SNeIa data sets respectively, as given in Table I of ref. [54]. The equivalent  $w_{TS}$  for the timescape model uses a void fraction  $f_{v0} = 0.76^{+0.12}_{-0.09}$  as determined in ref. [24].  $1\sigma$  uncertainties are listed in each case.

$z < 0.42$  when combined with 185 SNeIa from other surveys, yields best-fit parameters  $w = -0.96 \pm 0.06$  (syst)  $\pm$  0.12 (stat) and  $\Omega_{M0} = 0.265 \pm 0.016$  (syst)  $\pm$  0.025 (stat) using SALT-II to fit to spatially flat FLRW models with constant  $w$ , but  $w = -0.76 \pm 0.07$  (syst)  $\pm$  0.11 (stat) and  $\Omega_{M0} = 0.307 \pm 0.019$  (syst)  $\pm$  0.023 (stat) using MLCS2k2. Use of MLCS2k2 is therefore also likely to somewhat change the data values in Table I and Fig. 4.

At this stage the uncertainties, especially systematic ones in data reduction, are too large to draw firm conclusions, but future measurements may change the picture. Of course given specific models of dark energy, greater statistical leverage is obtained simply by comparing  $H_0 D$  directly on a model by model basis.

## B. Angular-size redshift relation

The angular size,  $\delta = \ell/d_A$ , of a class of objects of uniform proper length,  $\ell$ , is readily determined from (40), (41). Empirically the differences from the  $\Lambda$ CDM model are not very large. For the best-fit value  $f_{v0} = 0.762$  the minimum angle occurs at  $z = 1.74$ , as opposed to  $z = 1.67$  for a spatially flat  $\Lambda$ CDM model with  $\Omega_{M0} = 0.249$ , or  $z = 1.56$  for a spatially flat  $\Lambda$ CDM model with  $\Omega_{M0} = 0.34$ . The angle subtended by standard rulers in the timescape model is very slightly less than for the comparison spatially flat  $\Lambda$ CDM models. At  $z = 6$  the difference is of order 9–15%.

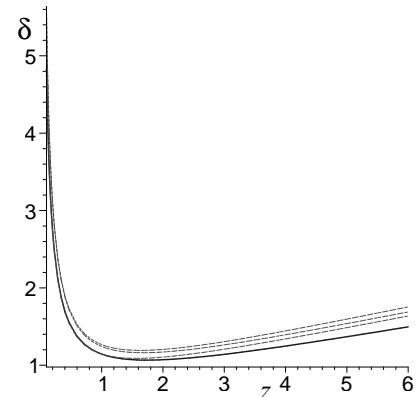


FIG. 5: The angle,  $\delta$  (in arcsec), subtended by a 10kpc source as a function of redshift for the timescape model with  $f_{v0} = 0.762$ ,  $H_0 = 61.7 \text{ km sec}^{-1} \text{ Mpc}^{-1}$  (solid line) as compared to the equivalent angular size relation for three spatially flat  $\Lambda$ CDM models (dashed lines from top to bottom): (a)  $(\Omega_{M0}, \Omega_{\Lambda0}) = (0.279, 0.721)$ ,  $H_0 = 71.9 \text{ km sec}^{-1} \text{ Mpc}^{-1}$ ; (b)  $(\Omega_{M0}, \Omega_{\Lambda0}) = (0.249, 0.751)$ ,  $H_0 = 71.9 \text{ km sec}^{-1} \text{ Mpc}^{-1}$ ; (c)  $(\Omega_{M0}, \Omega_{\Lambda0}) = (0.34, 0.66)$ ,  $H_0 = 62.7 \text{ km sec}^{-1} \text{ Mpc}^{-1}$ .

## IV. THE $H(z)$ AND $Om(z)$ MEASURES

Recently Sahni, Shafieloo and Starobinsky [58, 59] have proposed a new diagnostic of dark energy, the function

$$Om(z) \equiv \frac{\frac{H^2(z)}{H_0^2} - 1}{(1+z)^3 - 1}, \quad (47)$$

on account of the fact that it is equal to the constant present epoch matter density parameter,  $\Omega_{M0}$ , at all redshifts for a spatially flat FLRW model with pressureless dust and a cosmological constant, but is not constant if the cosmological constant is replaced by other forms of dark energy. For a spatially flat universe with pressureless dust plus some arbitrary dark energy one has

$$Om(z) = \Omega_{M0} + (1 - \Omega_{M0}) \frac{(1+z)^{3(1+w)} - 1}{(1+z)^3 - 1}. \quad (48)$$

For general FLRW models  $H = D'^{-1} \sqrt{1 + \Omega_{k0} H_0^2 D^2}$  only involves a single derivative of  $D(z)$ , and so the diagnostic (47) is easier to reconstruct observationally than the equation of state parameter,  $w(z)$ .

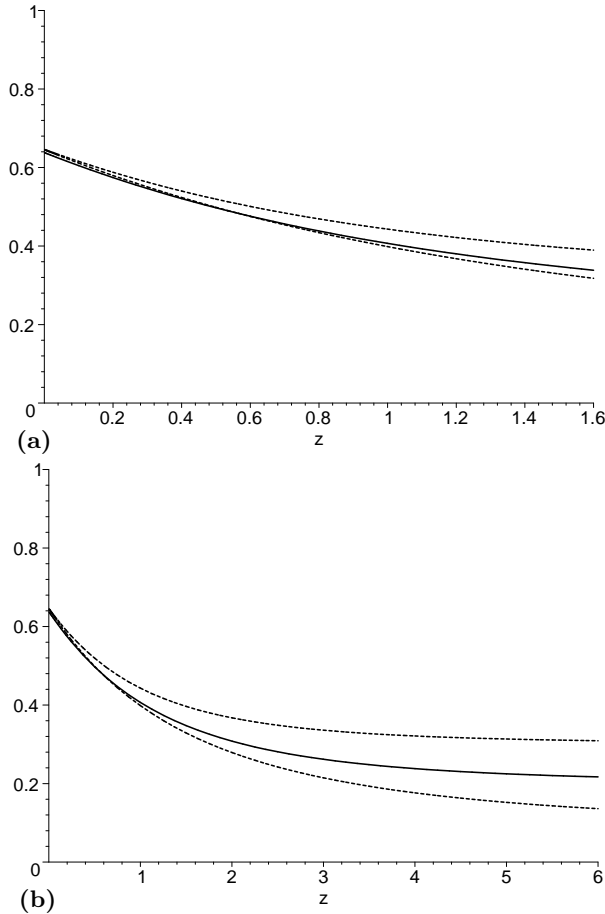


FIG. 6: The dark energy diagnostic  $Om(z)$  of Sahni, Shafieloo and Starobinsky [58] plotted for the timescape tracker solution with best-fit value  $f_{v0} = 0.762$  (solid line), and  $1\sigma$  limits (dashed lines) from ref. [24]: (a) for the redshift range  $0 < z < 1.6$  as shown in ref. [59]; (b) for the redshift range  $0 < z < 6$ .

The quantity  $Om(z)$  is readily calculated for the timescape model, and is shown in Fig. 6. What is striking about Fig. 6, as compared to the curves for quintessence and phantom dark energy models plotted in ref. [58], is that the initial value

$$Om(0) = \frac{2}{3} H'|_0 = \frac{2(8f_{v0}^3 - 3f_{v0}^2 + 4)(2 + f_{v0})}{(4f_{v0}^2 + f_{v0} + 4)^2} \quad (49)$$

is substantially larger than in the dark energy models. We note from (49) that  $\lim_{f_{v0} \rightarrow 0} Om(0) = 1$ , and  $\lim_{f_{v0} \rightarrow 1} Om(0) = \frac{2}{3}$ , with a minimum value of  $Om(0) \simeq 0.638$  at  $f_{v0} \simeq 0.774$ . The best-fit present epoch void fraction [24] gives a value of  $Om(0)$  very close to the minimum. For the range  $f_{v0} = 0.76^{+0.12}_{-0.9}$  [24]  $Om(0)$  is tightly constrained to the range  $0.638 < Om(0) < 0.646$ .

A further difference for the timescape model is that  $Om(z)$  does not asymptote to the dressed density parameter  $\Omega_{M0}$  in any redshift range. For quintessence models  $Om(z) > \Omega_{M0}$ , while for phantom models  $Om(z) < \Omega_{M0}$ , and in both cases  $Om(z) \rightarrow \Omega_{M0}$  as  $z \rightarrow \infty$ . In the timescape model,  $Om(z) > \Omega_{M0} \simeq 0.33$  for  $z \lesssim 1.7$ , while  $Om(z) < \Omega_{M0}$  for  $z \gtrsim 1.7$ . It thus behaves more like a quintessence model for low  $z$ , in accordance with Fig. 3. However, the steeper slope and the completely different behaviour at large  $z$  mean the diagnostic is generally very different to that of dark energy models. For large  $z$ ,

$$\lim_{z \rightarrow \infty} Om(z) = \frac{2(1 - f_{v0})(2 + f_{v0})^3}{(4f_{v0}^2 + f_{v0} + 4)^2}, \quad (50)$$

giving a value  $\bar{\Omega}_{M0} < Om(\infty) < \bar{\Omega}_{M0}$ , if  $f_{v0} > 0.25$ . For example for  $f_{v0} = 0.762$ , we find  $Om(\infty) \simeq 0.2$ .

Shafieloo, Sahni and Starobinsky [59] have recently tested the  $Om(z)$  statistic against CMB, BAO and SNeIa data, including the Constitution SNeIa data [56]. In comparing their results with Fig. 6 it should be noted that their analysis entails taking particular empirical functions for  $w(z)$ , and then best-fitting the free parameters. The two functions they choose are: (i)  $w(z) = w_0 + w_1 z / (1 + z)$ ; and (ii)  $w(z) = -\frac{1}{2}[1 + \tanh((z - z_t)\Delta)]$ , where  $w_0$ ,  $w_1$ ,  $z_t$  and  $\Delta$  are empirically fit constants. In both these cases  $w(z)$  is monotonic and cannot completely accommodate the equivalent ‘‘artificial dark energy equation of state’’ for the timescape model as depicted in Fig. 3 at large  $z$ . Furthermore, the effective  $w(z)$  of Fig. 3(a) becomes nonlinear in the range  $0.5 \lesssim z \lesssim 1$ , contradicting the parameterization of case (i) of [59]. Also, it crosses the ‘‘phantom divide’’ at  $z \simeq 0.464$  contradicting the parameterization of case (ii). However, we can expect that the empirical forms of  $w(z)$  assumed by Shafieloo *et al* to have some comparative value for the timescape model at very low values of  $z$ . The greatest leverage should come as  $z \rightarrow 0$ . It is therefore interesting to note that of the two empirical forms for  $w(z)$  assumed by Shafieloo *et al*, the one that provides the better fit, case (ii), gives a best-fit intercept  $Om(0)$  remarkably close to the expectation from (49) for  $f_{v0} = 0.762$ , viz.  $Om(0) = 0.638$ . (See Fig. 3 right hand panel of ref. [59].) Since this is not the expectation for either a typical quintessence or phantom energy model, it is an encouraging result for the timescape model, which is also consistent with the study of Zhao and Zhang [53].

Shafieloo *et al* have suggested [59] that their analysis of the recent data might give a hint that ‘‘dark energy is decaying’’. Given that the results of ref. [59] appear to be consistent with the expectations of the timescape model, our analysis sheds a different light on this interpretation. It should also be noted that a pure FLRW model with substantial negative spatial curvature, i.e., with  $\Omega_{k0} > 0$ , will give an intercept  $Om(0) = \Omega_{M0} + \frac{2}{3}\Omega_{k0}$ , whose value could assume a similar value to that obtained for the timescape model. Of course, this would require a value

of  $\Omega_{k0}$  which is ruled out by the WMAP analysis for the FLRW case, which is why such values have not been considered by Shafieloo *et al.* As observed above  $Om(0)$  has a very tight range of values for a wide range of reasonable values of  $f_{v0}$ . Thus if the tests of the  $Om(z)$  statistic could be improved to include a wider range of empirical  $w(z)$  functions, including those that more closely mimic our relation (45), then this would be an interesting test once significantly more data becomes available.

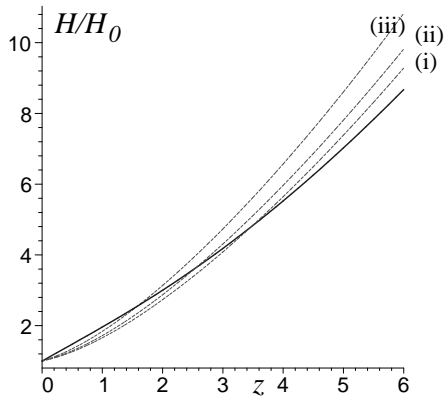


FIG. 7: The function  $H_0^{-1}H(z)$  for the timescape model with  $f_{v0} = 0.762$  (solid line) is compared to  $H_0^{-1}H(z)$  for three spatially flat  $\Lambda$ CDM models with the same values of  $(\Omega_{M0}, \Omega_{\Lambda0})$  as in Fig. 2 (dashed lines): (i)  $(\Omega_{M0}, \Omega_{\Lambda0}) = (0.249, 0.751)$ ; (ii)  $(\Omega_{M0}, \Omega_{\Lambda0}) = (0.279, 0.721)$ ; (iii)  $(\Omega_{M0}, \Omega_{\Lambda0}) = (0.34, 0.66)$ .

The strong differences seen in the  $Om(z)$  diagnostic between the timescape model and typical dark energy models might be seen to arise from the fact that it accentuates the differences which already exist in the dressed  $H(z)$  function, which is quite different to that of the Friedmann equation. Using (B9) we plot  $H(z)/H_0$  for the best-fit timescape model, and compare it to the spatially flat  $\Lambda$ CDM models that were plotted in Fig. 2. For  $z < 1.5$   $H(z)/H_0$  for the timescape model with  $f_{v0} = 0.762$  is greater than for the  $\Lambda$ CDM models shown. The absolute value of  $H(z)$  is partly compensated for, however, by the higher value of  $H_0$  that is generally assumed for the  $\Lambda$ CDM models.

Gaztañaga, Cabré and Hui [60] have recently given measurements of  $H(z)$  at three redshifts, inferred from the separation of radial and transverse BAO scales in the SDSS-DR6 data, as will be discussed in Sec. V. However, their values are model dependent, being estimated according to

$$H(z)_{\text{true}} = \frac{r_{\text{BAO}}}{r_{\text{WMAP}}} H_0 \sqrt{0.25(1+z)^3 + 0.75}$$

with a fiducial expansion rate for a spatially flat  $\Lambda$ CDM model, with  $\Omega_{M0} = 0.25$ , used to convert redshifts to distances. Any estimates of  $H(z)$  will inevitably involve some model dependence, unless one can perform a test

such as the time drift of cosmological redshifts, which will be discussed in Sec. VII.

## V. THE ALCOCK–PACZYŃSKI TEST AND BARYON ACOUSTIC OSCILLATIONS

Alcock and Paczyński devised a test [61] which relies on comparing the radial and transverse proper length scales of spherical standard volumes comoving with the Hubble flow [62]. This test was originally conceived to distinguish FLRW models with a cosmological constant from those without a  $\Lambda$  term. The test is free from many evolutionary effects, but relies on one being able to remove systematic distortions due to peculiar velocities.

For the timescape model the Alcock–Paczyński test function determined from the dressed geometry is

$$f_{\text{AP}} = \frac{1}{z} \left| \frac{\delta\theta}{\delta z} \right| = \frac{HD}{z} = \frac{3(2t^2 + 3bt + 2b^2)(1+z)d_A}{t(2t+3b)^2 z}, \quad (51)$$

where  $t$  is given implicitly in terms of  $z$  by (38).

In Fig. 8 the Alcock–Paczyński test function (51) is compared to that of spatially flat  $\Lambda$ CDM model with different values of  $(\Omega_{M0}, \Omega_{\Lambda0})$ . The curve for the timescape model has a distinctly different shape to those of the  $\Lambda$ CDM models, being convex. However, the extent to which the curves can be reliably distinguished would require detailed analysis based on the precision attainable with any particular experiment.

Current detections of the BAO scale in clustering statistics of LRGs [29]–[34] can in fact be viewed as a variant of the Alcock–Paczyński test, as they make use of both the transverse and radial dilations of the fiducial comoving BAO scale to present a measure

$$D_V = \left[ \frac{zD^2}{H(z)} \right]^{1/3} = D f_{\text{AP}}^{-1/3}. \quad (52)$$

In Fig. 9 the BAO radial test function (52) is compared to that of the same spatially flat  $\Lambda$ CDM models plotted in Fig. 8, for the same redshift ranges.

Although the  $D_V$  measure for the timescape model is significantly different to that of the  $\Lambda$ CDM model at the higher redshifts shown in Fig. 9(b), we see from Fig. 9(a) that at the nearby redshifts the  $D_V$  measure gives considerably less discriminatory leverage. A case in point is provided by the ratio  $r_{0.35:0.2} \equiv D_V(0.35)/D_V(0.2)$ , which has been determined observationally [30, 34]. In this case the timescape model with  $f_{v0} = 0.76_{-0.09}^{+0.12}$  gives  $r_{0.35:0.2} = 1.632_{-0.007}^{+0.005}$ , as compared to  $r_{0.35:0.2} = 1.664_{-0.007}^{+0.009}$  for a spatially flat  $\Lambda$ CDM model with  $\Omega_{M0} = 0.28 \pm 0.03$ ; values which are close. By comparison the observed ratio was initially estimated to be  $r_{0.35:0.2} = 1.812 \pm 0.060$  [30], but this estimate has recently been revised to  $r_{0.35:0.2} = 1.736 \pm 0.065$  [34].

In fact, one must exercise caution in comparing the prediction of  $r_{0.35:0.2}$  for the timescape model with the

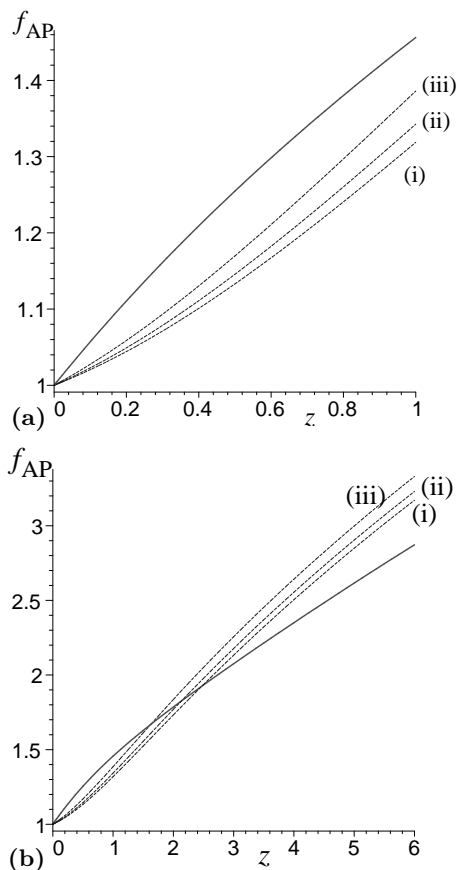


FIG. 8: The Alcock–Paczyński test function  $f_{\text{AP}} = \frac{1}{z} \left| \frac{\delta\theta}{\delta z} \right|$  for the timescape model with  $f_{\text{v}0} = 0.762$  (solid line) is compared to  $f_{\text{AP}}$  for three spatially flat  $\Lambda$ CDM models with the same values of  $(\Omega_{M0}, \Omega_{\Lambda0})$  as in Fig. 2 (dashed lines): (i)  $(\Omega_{M0}, \Omega_{\Lambda0}) = (0.249, 0.751)$ ; (ii)  $(\Omega_{M0}, \Omega_{\Lambda0}) = (0.279, 0.721)$ ; (iii)  $(\Omega_{M0}, \Omega_{\Lambda0}) = (0.34, 0.66)$ . Two redshift ranges are shown: (a)  $0 < z < 1$ ; (b)  $0 < z < 6$ .

“observed” ratio [30, 34] since the galaxy clustering data has been analysed in a manner which assumes an underlying FLRW model. The relevant analyses [30, 34] involve transformations to Fourier space to treat the power spectrum. To revisit such an analysis for the timescape model is far from trivial, as it requires a recalibration of transfer functions, and of the cosmological drag epoch,  $z_d$ , for a rather different cosmological parameterization given that we are dealing with a model which does not evolve as a homogeneous isotropic cosmology. In particular, the mass ratio of nonbaryonic dark matter to baryonic matter can be somewhat different [24] from the concordance  $\Lambda$ CDM model, and this needs to be considered. Given that the difference in the value of  $r_{0.35:0.2}$  quoted between refs. [30] and [34] is due to changes in the manner in which the data is treated, as well as the fact that there is more data, it is clear the differences in calibration due to a change of the nonbaryonic to baryonic mass ratio could also similarly affect the value of the “observed” ratio.

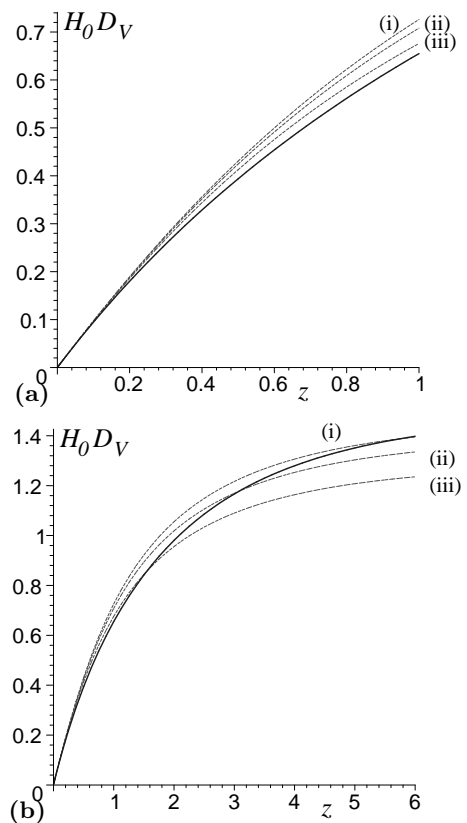


FIG. 9: The BAO radial test function  $H_0 D_V = H_0 D f_{\text{AP}}^{-1/3}$  for the timescape model with  $f_{\text{v}0} = 0.762$  (solid line) is compared to  $H_0 D_V$  for three spatially flat  $\Lambda$ CDM models with the same values of  $(\Omega_{M0}, \Omega_{\Lambda0})$  as in Fig. 2 (dashed lines): (i)  $(\Omega_{M0}, \Omega_{\Lambda0}) = (0.249, 0.751)$ ; (ii)  $(\Omega_{M0}, \Omega_{\Lambda0}) = (0.279, 0.721)$ ; (iii)  $(\Omega_{M0}, \Omega_{\Lambda0}) = (0.34, 0.66)$ . Two redshift ranges are shown: (a)  $0 < z < 1$ ; (b)  $0 < z < 6$ .

A derivation of tools which would enable us to perform the BAO tests to the extent of refs. [30, 34] is beyond the scope of the present paper. Instead, it is our aim to simply explore what the best possible discriminating tests will be. In this regard, we note that if we compare Fig. 8(a) and Fig. 9(a), then it is clear that the Alcock–Paczyński test provides much more significant differences between the timescape model and  $\Lambda$ CDM models than the  $D_V$  measure. In fact, the  $D_V$  measure is currently employed because there is not yet sufficient data to separately estimate both the radial and transverse BAO signals directly, as would be required for the Alcock–Paczyński test.

Gaztañaga, Cabré and Hui [60] have recently claimed to separate the radial and angular scales corresponding to the BAO in the 2–point correlation function, by assuming a nonlinear gravitational lensing magnification bias. Using SDSS-DR6 data they have exhibited a correlation function in both the radial and transverse dimensions, for redshift slices at  $z = 0.15\text{--}0.30$  and at  $z = 0.40\text{--}0.47$ . They have not yet provided separate estimates of both the radial and transverse BAO scales. However, pro-

redshift range	$\Omega_{M0}h^2$	$\Omega_{B0}h^2$	$\Omega_{C0}/\Omega_{B0}$
0.15-0.30	0.132	0.028	3.7
0.15-0.47	0.12	0.026	3.6
0.40-0.47	0.124	0.04	2.1

TABLE II: Values of  $\Omega_{M0}h^2$ ,  $\Omega_{B0}h^2$  inferred by Gaztañaga, Cabré and Hui [60], and the resulting mass ratio of nonbaryonic dark matter to baryonic matter,  $\Omega_{C0}/\Omega_{B0}$ .

vided their techniques are robust, then a direct Alcock–Paczynski test may soon be on the horizon. Naturally such estimates will have model dependence. From the the point of view of the timescape model, one must carefully consider not only the treatment of redshift space distortions, but also any assumptions which rely on calibrations of FLRW models, as discussed above.

One point of the analysis of Gaztañaga, Cabré and Hui is suggestive. They find some tension between their best-fit value of the baryon density parameter  $\Omega_{B0} \simeq 0.06$  and the WMAP5 value [28]  $\Omega_{B0} \simeq 0.0432$ . The discrepancy is greater in the higher redshift slice. Their results are summarized in Table II. The inferred values for the mass ratio of nonbaryonic dark matter to baryonic matter of  $\Omega_{C0}/\Omega_{B0} = (\Omega_{M0} - \Omega_{B0})/\Omega_{B0}$  are 3.6 in the whole sample, 3.7 in the lower  $z$  slice and 2.1 in the higher  $z$  slice, as compared to the expectation of a ratio of 6.1 from WMAP5, for which  $(\Omega_{B0}h^2, \Omega_{M0}h^2) = (0.0227, 0.1308)$  [28]. In other words, the best-fit values indicate a somewhat higher mass fraction of baryons than the fit to WMAP5 with a FLRW model. This is confirmed by analysis of the 3-point correlation function [63], and is a feature which the authors find difficult to explain as a systematic error. The analysis of the 3-point function yields a best fit [63]  $\Omega_{M0} = 0.28 \pm 0.05$ ,  $\Omega_{B0} = 0.079 \pm 0.025$ .

For the timescape model by comparison, analysis of the Riess07 gold data [24, 64] yields dressed parameters  $\Omega_{M0} = 0.33^{+0.11}_{-0.16}$ ,  $\Omega_{B0} = 0.080^{+0.021}_{-0.013}$ , and a ratio  $\Omega_{C0}/\Omega_{B0} = 3.1^{+2.5}_{-2.4}$  from supernovae alone. Demanding a fit of the angular diameter distance of the sound horizon [14] to within 4% would reduce these bounds to  $\Omega_{C0}/\Omega_{B0} = 3.1^{+1.8}_{-1.3}$  for the timescape model. Thus the higher baryon density indicated by the analysis of Gaztañaga, Cabré and Hui is consistent with the expectations of the timescape model.

Finally, we note that although the reality of the BAO measure is accepted by most researchers [29]–[36], Sylos Labini *et al* [45] have questioned this. Although Sylos Labini *et al* detect the BAO scale in the LRG sample, they point out that its amplitude is less than the overall density variations of 8% at large scales, and furthermore the correlation function remains positive where the  $\Lambda$ CDM model predicts it should be negative. Sample uncertainties may limit the strength of this conclusion [35], however.

In my view, although the results of ref. [45] may poten-

tially indicate problems with a statistical analysis based on the expectations of a FLRW cosmology, the BAO is a real feature which will survive despite the observed inhomogeneities. The point is that given a universe which was very close to homogeneous and isotropic at last scattering, it can only evolve so far away from homogeneity in the time available since that epoch. Thus there is every reason to expect that statistical analyses of the type that are being performed can pick up a feature in the two-point correlation function, even if there are larger scale variations in density of order 8%. The exact properties of the statistical correlation functions within a framework such as the timescape cosmology await a detailed analysis. The main difference is that the density of the observable universe when measured on scales larger than that of “statistical homogeneity” will retain some intrinsic variance, and furthermore is not the time-evolution of the mean density of the statistical ensemble at last scattering. This is likely to have important consequences for the statistical analysis.

## VI. TEST OF (IN)HOMOGENEITY

Recently Clarkson, Bassett and Lu [65] have constructed what they call a “test of the Copernican principle” based on the observation that for homogeneous, isotropic models which obey the Friedmann equation, the present epoch curvature parameter, a constant, may be written as

$$\Omega_{k0} = \frac{[H(z)D'(z)]^2 - 1}{[H_0D(z)]^2} \quad (53)$$

for all  $z$ , irrespective of the dark energy model or any other model parameters. Consequently, taking a further derivative, the quantity

$$\mathcal{C}(z) \equiv 1 + H^2(DD'' - D'^2) + HH'DD' \quad (54)$$

must be zero for all redshifts for any FLRW geometry.

A deviation of  $\mathcal{C}(z)$  from zero, or of (53) from a constant value, would therefore mean that the assumption of homogeneity is violated. Clarkson, Bassett and Lu refer to this as a “violation of the Copernican principle”. Given the viewpoint outlined in ref. [14], simply associating FLRW models with the Copernican principle is too great a restriction on its general philosophy. One should distinguish the Copernican Principle, which is generally understood as the statement that we do not occupy a privileged position in the universe, from the Cosmological Principle that the universe is described by a spatially homogeneous isotropic geometry.

In the presence of inhomogeneity there can still be statistically average cells – taken here to be of size  $100h^{-1}$  Mpc – but with a variance of the geometry within such cells. As observers in an average galaxy, our position is unremarkable from the point of view of the Copernican principle. Nonetheless, the local geometry in an average void can be markedly different from the geometry in

an average galaxy. Given that observers and the things they observe are necessarily in bound structures, structure formation provides a selection effect in terms of our local geometry vis-à-vis the volume-average geometry in a void. Given this improved understanding of the Copernican principle, one should not call the test of Clarkson, Bassett and Lu a test of the Copernican principle. It is simply a test of the validity of the FLRW models.

Since the timescape model is inhomogeneous, it will certainly violate the test of Clarkson, Bassett and Lu. If one can determine  $H(z)$  in a model independent way, then tests of relations (53) or (54) could not only rule on whether the FLRW model is violated, but also test the timescape model. Analytic expressions for  $HD'$  and  $HD''$  are obtained by multiplying (53) and (54) by (B8). Combining the results with (40) and (B11) we find that (53) becomes

$$\Omega_{k0} = \frac{\mathcal{B}(z)}{H_0^2(1+z)^2 d_A^2} \quad (55)$$

where

$$\mathcal{B} = \frac{(2t-b)d_A}{(2t+3b)^2} \left[ 2 + \frac{(2t-b)d_A}{(2t+3b)^2} \right] \quad (56)$$

while (54) becomes

$$\mathcal{C} = -\frac{(2t-b)d_A}{(2t+3b)^2} - \frac{3b(10t^2 + 11bt - 2b^2)d_A^2}{t(2t+3b)^4}. \quad (57)$$

Once again,  $d_A$  is given by (40) and  $t$  is given implicitly in terms of  $z$  via (38).

We plot the functions  $\mathcal{B}(z)$  and  $\mathcal{C}(z)$  in Figs. 10 and 11. The function  $\mathcal{C}$  differs appreciably from the FLRW value of zero. However, two derivatives are required to determine  $\mathcal{C}(z)$ , which is subject to greater uncertainties for actual data, given that  $D(z)$  is effectively what is measured. Thus it would be more feasible to determine  $\mathcal{B}(z) = [HD']^2 - 1$ , which involves a single derivative of the observed curve. (It makes more sense to plot  $\mathcal{B}(z)$ , rather than the right hand side of eq. (53), which involves a division by zero as  $z \rightarrow 0$ .) In Fig. 10  $\mathcal{B}(z)$  for the timescape model is compared to the expectations for  $\Lambda$ CDM models with a small amount of spatial curvature, as compatible with WMAP. The form of  $\mathcal{B}(z)$  is very different at small redshifts, which suggests that this will be a useful observational test. Furthermore, since  $\mathcal{B}(z)$  has a maximum value and also changes sign, its form for the timescape model is very different to that of any FLRW model. In the FLRW case  $\mathcal{B}(z)$  is always a monotonic function whose sign is determined by that of  $\Omega_{k0}$ . At large  $z$ , or equivalently at early times as  $t \rightarrow 0$ ,  $\mathcal{B}(z) \rightarrow 0$  and  $\mathcal{C}(z) \rightarrow 0$  for the timescape model, consistent with the fact that it coincides with a spatially flat Einstein-de Sitter universe at early times. Since  $\mathcal{C}(z)$  involves second derivatives, it goes to zero more slowly than  $\mathcal{B}(z)$ : for the best-fit solution of Figs. 10 and 11,  $\mathcal{B}(1100) \simeq -0.0029$ , while  $\mathcal{C}(1100) \simeq 0.075$ .

It is interesting to compare Fig. 11 with the corresponding plot of  $\mathcal{C}(z)$  for a LTB model with a large void recently given in Fig. 14 of ref. [66]. The magnitude of  $\mathcal{C}(z)$  is considerably larger for the timescape model.

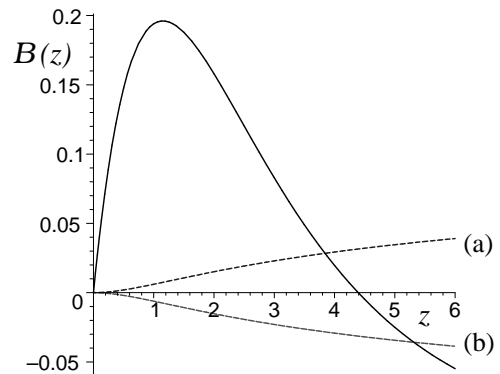


FIG. 10: The homogeneity test function  $\mathcal{B}(z) = [HD']^2 - 1$  is plotted for the timescape tracker solution with best-fit value  $f_{v0} = 0.762$  (solid line), and compared to the equivalent curves  $\mathcal{B} = \Omega_{k0}(H_0 D)^2$  for two different  $\Lambda$ CDM models with small curvature: (a)  $\Omega_{M0} = 0.28$ ,  $\Omega_{\Lambda0} = 0.71$ ,  $\Omega_{k0} = 0.01$ ; (b)  $\Omega_{M0} = 0.28$ ,  $\Omega_{\Lambda0} = 0.73$ ,  $\Omega_{k0} = -0.01$ . A spatially flat FLRW model would have  $\mathcal{B}(z) \equiv 0$ .

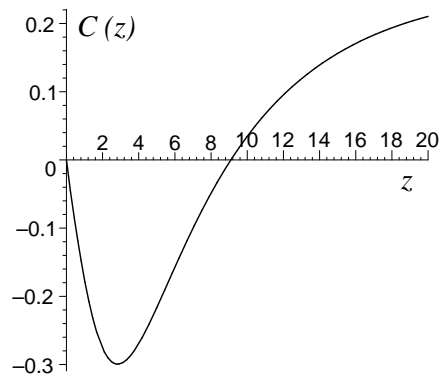


FIG. 11: The homogeneity test function  $\mathcal{C}(z)$  given by (54) is plotted for the timescape tracker solution with best-fit value  $f_{v0} = 0.762$ . Any FLRW model would have  $\mathcal{C}(z) \equiv 0$ , regardless of its spatial curvature.

## VII. TIME DRIFT OF COSMOLOGICAL REDSHIFTS

For the purpose of the (in)homogeneity test considered in the last section,  $H(z)$  must be observationally determined, and this is difficult to achieve in a model independent way. There is one way of achieving this, however, namely by measuring the time variation of the redshifts of different sources over a sufficiently long time interval [67], as has been discussed recently in relation to tests of (in)homogeneity by Uzan, Clarkson and Ellis

[68]. Although the measurement is extremely challenging, it may be feasible over a 20 year period by precision measurements of the Lyman- $\alpha$  forest in the redshift range  $2 < z < 5$  with the next generation of Extremely Large Telescopes [69].

For FLRW models one has

$$\frac{dz}{dt} = H_0(1+z) - H(z) \quad (58)$$

which in the case of a  $\Lambda$ CDM model with possible spatial curvature leads directly to

$$\frac{1}{H_0} \frac{dz}{dt} = (1+z) - \sqrt{\Omega_{M0}(1+z)^3 + \Omega_{\Lambda0} + \Omega_{k0}(1+z)^2}. \quad (59)$$

For the timescape model one has an expression identical to (58) in terms of the dressed Hubble parameter if the time derivative is taken with respect to wall time,  $\tau$ . Using (B8) we find that

$$\begin{aligned} \frac{1}{H_0} \frac{dz}{d\tau} &= 1+z - \frac{H}{H_0} \\ &= 1+z - \frac{3(2t^2 + 3bt + 2b^2)}{H_0 t(2t + 3b)}, \end{aligned} \quad (60)$$

where  $t$  is given implicitly in terms of  $z$  by (38).

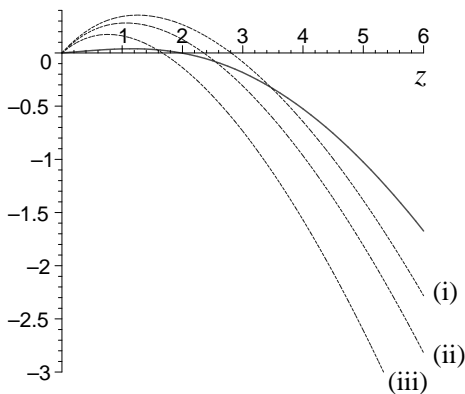


FIG. 12: The function  $H_0^{-1} \frac{dz}{d\tau}$  for the timescape model with  $f_{v0} = 0.762$  (solid line) is compared to  $H_0^{-1} \frac{dz}{dt}$  for three spatially flat  $\Lambda$ CDM models with the same values of  $(\Omega_{M0}, \Omega_{\Lambda0})$  as in Fig. 2 (dashed lines): (i)  $(\Omega_{M0}, \Omega_{\Lambda0}) = (0.249, 0.751)$ ; (ii)  $(\Omega_{M0}, \Omega_{\Lambda0}) = (0.279, 0.721)$ ; (iii)  $(\Omega_{M0}, \Omega_{\Lambda0}) = (0.34, 0.66)$ .

In Fig. 12 we compare  $H_0^{-1} \frac{dz}{d\tau}$  for the best-fit timescape model with  $f_{v0} = 0.762$  to the equivalent function for three different spatially flat  $\Lambda$ CDM models. What is notable is that the curve for the timescape model is considerably flatter than those of the  $\Lambda$ CDM models. The origin of this feature may be understood qualitatively to arise from the fact that the magnitude of the apparent acceleration is considerably smaller in the timescape model, as compared to the magnitude of the acceleration

in  $\Lambda$ CDM models. For models in which there is no apparent acceleration whatsoever, one finds that  $H_0^{-1} \frac{dz}{d\tau}$  is always negative. If there is cosmic acceleration, real or apparent, at late epochs then  $H_0^{-1} \frac{dz}{d\tau}$  will become positive at low redshifts, though at a somewhat larger redshift than that at which acceleration is deemed to have begun.

Fig. 12 demonstrates that a very clear signal of differences in the redshift time drift between the timescape model and  $\Lambda$ CDM models might be determined at low redshifts when  $H_0^{-1} \frac{dz}{d\tau}$  should be positive. In particular, the magnitude of  $H_0^{-1} \frac{dz}{d\tau}$  is considerably smaller for the timescape model as compared to  $\Lambda$ CDM models. Observationally, however, it is expected that measurements will be best determined for sources in the Lyman  $\alpha$  forest in the range,  $2 < z < 5$ . At such redshifts the magnitude of the drift is somewhat more pronounced in the case of the  $\Lambda$ CDM models. For a source at  $z = 4$ , over a period of  $\delta\tau = 10$  years we would have  $\delta z = -3.3 \times 10^{-10}$  for the timescape model with  $f_{v0} = 0.762$  and  $H_0 = 61.7 \text{ km sec}^{-1} \text{ Mpc}^{-1}$ . By comparison, for a spatially flat  $\Lambda$ CDM model with  $H_0 = 70.5 \text{ km sec}^{-1} \text{ Mpc}^{-1}$  [28] a source at  $z = 4$  would over ten years give  $\delta z = -4.7 \times 10^{-10}$  for  $(\Omega_{M0}, \Omega_{\Lambda0}) = (0.249, 0.751)$ , and  $\delta z = -7.0 \times 10^{-10}$  for  $(\Omega_{M0}, \Omega_{\Lambda0}) = (0.279, 0.721)$ .

## VIII. DISCUSSION

In conclusion, the combination of tests we have described here have the potential to decide between the timescape cosmology, the  $\Lambda$ CDM cosmology, and other homogeneous isotropic cosmologies with other sources of dark energy. A number of the tests have been devised by other researchers with homogeneous dark energy cosmologies in mind. In these cases, the results of independent analyses performed to date are encouraging for the timescape model. In particular,

- A study of  $w(z)$  from recent datasets by Zhao and Zhang [53] provides mild evidence at the 95% confidence level for an effective  $w(z)$  which crosses the “phantom divide” near the redshift  $z \simeq 0.46$  indicated in Fig. 3(a), with  $w(z) + 1$  of the same sign over the relevant redshift ranges for  $z \lesssim 1$ ;
- Fits of classes of empirical  $w(z)$  functions by Shafieloo, Sahni and Starobinsky [59] yield, in the best-fit case, an  $Om(z)$  function with intercept  $Om(0)$  which appears to coincide with the timescape expectation,  $Om(0) \simeq 0.64$ ;
- Studies of the BAO scale in SDSS-DR6 data by Gaztañaga *et al* [60, 63] yield a relative mass fraction of baryonic matter to nonbaryonic dark matter, which is higher than the WMAP5 expectation with a FLRW cosmology, but which is perfectly consistent with the timescape model fit to the angular scale of the sound horizon [24].

While one can conceive of dark energy models with a  $w(z)$  which mimics Fig. 3(a) at redshifts  $z \lesssim 1$ , there is no reason to expect a different normalization of  $\Omega_{C0}/\Omega_{M0}$  for such models. Indeed primordial nucleosynthesis bounds are a very strong constraint on all cosmological models. It is precisely because the mean CMB temperature at a volume-average location unbound to physical structures in a void is cooler in the timescape scenario than the mean temperature we measure in a galaxy, that a different normalization of the primordial baryon-to-photon ratio relative to present epoch cosmological parameters is obtained. This would not be true for any homogeneous isotropic cosmology, regardless of the type of dark energy fluid.

Other future tests discussed in this paper also have definitive predictions. The expectation for the (in)homogeneity test of Clarkson, Bassett and Lu [65], yields a diagnostic  $\mathcal{B}(z)$  which is both distinctively different from FLRW models with spatial curvature as shown in Fig. 10, and from LTB models. The time-drift of cosmological redshifts would be most definitively tested by monitoring as many redshifts as possible in the range  $1 \lesssim z \lesssim 2$ . As shown in Fig. 12, in this range  $H_0^{-1} \frac{dz}{d\tau}$  should be very close to zero, and only very marginally positive as compared to the  $\Lambda$ CDM expectation. In the redshift range,  $2 \lesssim z \lesssim 5$ , which is expected to be the range most readily tested with the next generation of extremely large telescopes, the function  $H_0^{-1} \frac{dz}{d\tau}$  will have a flatter  $z$ -dependence for the timescape model than comparable  $\Lambda$ CDM models, as is seen in Fig. 12. The redshift range  $2 \lesssim z \lesssim 8$  can also be tested by GRB Hubble diagrams, and initial investigations are in progress [51].

This paper has considered tests on scales greater than that of statistical homogeneity. There are many other such tests in addition to those which we have discussed. A number of these involve the CMB, such as the determination of the amplitude of the late-time integrated Sachs-Wolfe effect. Such tests require first a computation of the detailed structure of the CMB acoustic peaks, recalibrated to the timescape cosmology. This is a very complicated task, which is why it has not been attempted here. However, it is an important goal for future work.

Below the scale of statistical homogeneity we expect to see apparent variance in the Hubble parameter, with a peak value 17% larger than the dressed global average value, measured over the scale of the dominant void fraction of  $30h^{-1}$  Mpc. Since voids dominate by volume, a spherically symmetric average out to a fixed redshift will yield generally higher values until we average over volumes for which a typical line of sight intersects as many walls and voids as the global average. That is, the spherically averaged Hubble parameter should decrease from a maximum at the  $30h^{-1}$  Mpc scale to the global average value at roughly the  $100h^{-1}$  Mpc scale. This general pattern is indeed borne out by the analysis of Li and Schwarz [20]. Much more detailed predictions of the expected variance could be made for the timescape model, by performing Monte Carlo simulations assuming a rea-

sonable distribution of voids and minivoids packed into  $100h^{-1}$  Mpc spheres. This is an important goal for future work, as it would give a Hubble bubble feature with unique characteristics, providing a test of a feature for which there is no counterpart in the standard cosmology.

The recent determination of  $H_0 = 74.2 \pm 3.6 \text{ km sec}^{-1} \text{ Mpc}^{-1}$  by the SH0ES survey [70] does provide a challenge for the timescape model. However, as we have just noted, in the timescape scenario spatial curvature gradients and apparent variance in the Hubble flow below the scale of statistical homogeneity introduce systematic issues which complicate the determination of  $H_0$ . Riess *et al* [70] have done a very careful analysis, and make efforts to account for a Hubble bubble – which they cut off at  $z = 0.023$ , approximately two thirds of the scale of statistical homogeneity. However, while they do not use supernovae with  $z < 0.023$  in the measurement of the Hubble flow, their calibration of the distance ladder is necessarily made on nearby scales, in particular using the maser distance to NGC 4258, at  $7.2 \pm 0.5$  Mpc, as an anchor. In the timescape scenario the effects of spatial inhomogeneity and spatial curvature gradients are greatest on scales up to  $30h^{-1}$  Mpc. Given that our own galaxy appears to be in a filament, this may have an impact in calibrating standard candles in the distance ladder.

The megamaser project [71] will therefore provide an interesting test, as it will yield purely geometric distances – independent of standard candle calibrations – on scales much larger than has been tested to date [72]. The relevant scales are considered to be well into the Hubble flow in the standard cosmology, and if distances of order  $\sim 60/h$  Mpc could be measured, would represent a substantial up to a large fraction of the scale of statistical homogeneity. The expectation in the timescape scenario is that provided such sources are sampled in directions in which the line of sight passes through a variety of different density fields, then there should be variance in the values of the Hubble constant so derived. The sample of maser distances required to test the statistical expectations of the timescape scenario would be considerably larger than the ten or so masers currently under investigation, but may become feasible in coming decades.

In comparing future measurements with model predictions it is important not only to extend the timescape model to develop counterparts of all the standard tests of the FLRW models, but also to carefully examine the methods by which astronomical data is reduced, as in many cases the standard cosmology is either explicitly or implicitly assumed. As one case in point, BAO analyses at present typically use a transformation to Fourier space and the use of spectral transfer functions calibrated to the FLRW models. Thus while the results of Gaztañaga *et al* [60, 63] are suggestive in that they find results in agreement with our expected  $\Omega_{C0}/\Omega_{B0}$  – which is the physical parameter responsible for the degree of baryon drag in the primordial plasma – in applying results of independent analyses to the timescape model one must exercise

caution until each step in the BAO data reduction is understood directly from calibrations with the timescape model.

Another important case in which data reduction must be carefully considered is that of supernovae. It was recently pointed out [73] that on Bayesian evidence the timescape model is disfavoured as compared to the  $\Lambda$ CDM model using the Union [55] and Constitution [56] compilations. However, the Union and Constitution data sets have been reduced using the SALT method in which one simultaneously marginalizes over both empirical light curve parameters and cosmological parameters, assuming a FLRW cosmology. Hicken *et al* [56] discuss and compare four different methods of data reduction: SALT, SALT2, MLCS31 and MLCS17. They find some systematic differences between the methods; for example, the SALT methods give larger scatter at higher redshifts.

As will be discussed in a forthcoming paper [74], use of the MLCS17 reduced data gives a different picture to the conclusions drawn by Kwan, Francis and Lewis [73]. In particular, analysis of the MLCS17-reduced 372 Snela of Hicken *et al* gives Bayesian evidence which favours the timescape model over the  $\Lambda$ CDM model. Thus there are already enough supernovae in principle to distinguish between the models; except that systematic uncertainties in the empirical methods by which standard candles are standardized at present limit the conclusions that can be drawn. Such issues are likely to also be a feature of many other astrophysical observations, and thus it is important that as many independent tests as possible are devised, and carried out carefully in a way in which any model-dependent assumptions are scrutinized.

It is hoped that the tests discussed in this paper will provide a basis for comparing the  $\Lambda$ CDM model with a physically well-grounded competing cosmological model. To fully compete, much further development of the timescape model is of course required. The standard cosmology consists of a base model for expansion of the universe – the FLRW model dating from the 1920s – on top of which a sophisticated superstructure has been built over the last few decades. This superstructure including features such as the generation of initial conditions from inflation, the bottom-up hierarchical structure formation process, and the results of large-scale structure simulations using Newtonian gravity on top of the base expansion. The model of refs. [14, 15] replaces the base expansion of the FLRW model by an average expansion which is not based on the Friedmann equation, and this paper has explored a number of tests which can be performed based solely on the average geometrical properties.

Many current cosmological tests of the standard cosmology – including detailed analysis of the CMB, galaxy clustering, redshift space distortions and weak lensing – can only be extended to the timescape model once the standard cosmology superstructure built on top of the FLRW model is adapted to the timescape model to understand the growth of structure at a more detailed level. Although this may seem a daunting task, it is perhaps

not as quite a tall order as one might at first think. In particular, the differences from a standard FLRW model with inflationary initial conditions at last scattering are negligible, and consequently many large portions of the standard cosmology would not change. In particular, the mechanisms of physical processes are largely still the same, but what does change is the relationship of present average cosmological parameters to the initial perturbations. Rederivation of the standard cosmology superstructure may largely be an issue of recalibration. Where the calculations involve transfer functions that relate initial perturbation spectra to their time evolved distributions, such recalibrations may be quite nontrivial, however. Thus a careful first principles re-examination is required. This is left to future work.

**Acknowledgements** I would like to thank Teppo Mattsson, Ishwaree Neupane and Peter Smale for discussions, and Jim Braatz, Thomas Buchert, Chris Clarkson, Francesco Sylos Labini and Brad Schaefer for correspondence. I also warmly thank Prof. Remo Ruffini and ICRA Net for support and hospitality while the bulk of the paper was completed. This work was also partly supported by the Marsden fund of the Royal Society of New Zealand.

## APPENDIX A: GENERAL TWO-SCALE SOLUTION TO THE BUCHERT EQUATIONS

The general solution for the two-scale [75] Buchert equations (16), (17) for the independent functions  $\bar{a}(t)$  and  $f_v(t)$  is given implicitly by [15]

$$(1 - f_v)^{1/3} \bar{a} = \bar{a}_0 \left[ (1 - \epsilon_i) \bar{\Omega}_{M0} \right]^{1/3} \left( \frac{3}{2} \bar{H}_0 t \right)^{2/3}, \quad (\text{A1})$$

$$\sqrt{u(u + C_\epsilon)} - C_\epsilon \ln \left( \left| \frac{u}{C_\epsilon} \right|^{\frac{1}{2}} + \left| 1 + \frac{u}{C_\epsilon} \right|^{\frac{1}{2}} \right) = \frac{\alpha}{\bar{a}_0} (t + t_\epsilon), \quad (\text{A2})$$

where  $u \equiv f_v^{1/3} \bar{a} / \bar{a}_0 = f_{vi}^{1/3} a_v / \bar{a}_0$  is proportional to  $a_v$ ;  $C_\epsilon \equiv \epsilon_i \bar{\Omega}_{M0} f_{v0}^{1/3} / \bar{\Omega}_{k0}$ ;  $\alpha \equiv \bar{a}_0 \bar{H}_0 \bar{\Omega}_{k0}^{1/2} / f_{v0}^{1/6}$ ;  $\epsilon_i$  and  $t_\epsilon$  being constants of integration, while  $f_{v0}$ ,  $\bar{H}_0$ ,  $\bar{\Omega}_{M0}$  and  $\bar{\Omega}_{k0}$  are the present epoch values of  $f_v$ ,  $\bar{H}$ ,  $\bar{\Omega}_M$  and  $\bar{\Omega}_k$  respectively. Since  $f_{wi}^{1/3} a_w = (1 - f_v)^{1/3} \bar{a}$ , Eq. (A1) may also be written as  $a_w = a_{w0} t^{2/3}$ , where  $a_{w0} \equiv \bar{a}_0 \left[ \frac{9}{4} f_{wi}^{-1} (1 - \epsilon_i) \bar{\Omega}_{M0} \bar{H}_0^2 \right]^{1/3}$ .

The lapse function,  $\bar{\gamma}$ , bare matter density parameter,  $\bar{\Omega}_M$ , and void fraction,  $f_v$ , satisfy the integral constraint

$$\frac{(1 - \epsilon_i) \bar{\gamma}^2 \bar{\Omega}_M}{(1 - f_v)} = 1. \quad (\text{A3})$$

Furthermore,  $H_w = 2/(3t)$ , while  $H_v = H_w/h_r$  where

$$h_r = \sqrt{\frac{(1 - \epsilon_i)\bar{\Omega}_{M0}f_{v0}^{1/3}f_v}{(\bar{\Omega}_{k0}u + \bar{\Omega}_{M0}f_{v0}^{1/3}\epsilon_i)(1 - f_v)}}. \quad (\text{A4})$$

Of the six constants  $\epsilon_i$ ,  $t_\epsilon$ ,  $f_{v0}$ ,  $\bar{H}_0$ ,  $\bar{\Omega}_{M0}$  and  $\bar{\Omega}_{k0}$ , only four are independent since there are additional constraints [15]

$$\sqrt{(1 - \epsilon_i)\bar{\Omega}_{M0}(1 - f_{v0})} + \sqrt{(\bar{\Omega}_{k0} + \bar{\Omega}_{M0}\epsilon_i)f_{v0}} = 1 \quad (\text{A5})$$

$$\frac{\bar{\Omega}_{k0}^{3/2}}{f_{v0}^{1/2}}\bar{H}_0(t_0 + t_\epsilon) = \sqrt{\bar{\Omega}_{k0}(\bar{\Omega}_{k0} + \bar{\Omega}_{M0}\epsilon_i)}$$

$$-\bar{\Omega}_{M0}\epsilon_i \ln \left[ \sqrt{\left| \frac{\bar{\Omega}_{k0}}{\bar{\Omega}_{M0}\epsilon_i} \right|} + \sqrt{\left| 1 + \frac{\bar{\Omega}_{k0}}{\bar{\Omega}_{M0}\epsilon_i} \right|} \right], \quad (\text{A6})$$

where the age of the universe in volume-average time is

$$t_0 = \frac{2}{3\bar{H}_0} \sqrt{\frac{1 - f_{v0}}{(1 - \epsilon_i)\bar{\Omega}_{M0}}}, \quad (\text{A7})$$

on account of (A1).

Of the four independent parameters, two can be eliminated by demanding priors at the surface of last scattering which are consistent with the evidence of the CMB. The redshift of the surface of last scattering relative to wall observers at the present epoch,  $z \simeq 1100$ , is fixed by the ratio of our locally measured CMB temperature relative to the temperature scale of matter-radiation decoupling and recombination, which is for the most part determined by the binding energy of hydrogen. We require that the velocity perturbations and density perturbations at this epoch when  $z \simeq 1100$  are consistent with observation. For example, we can fix velocity perturbations by

demanding  $1 - h_{ri} \simeq 10^{-5}$  and density perturbations by restricting  $f_{vi}$ . Physically,  $f_{vi}$  is to be understood as the fraction of our present horizon volume,  $\mathcal{H}$ , which by cosmic variance was in uncompensated underdense perturbations at last scattering. If this uncompensated fraction is viewed as a single density perturbation then

$$\delta_{\mathcal{H}} \equiv \left( \frac{\delta\rho}{\rho} \right)_{\mathcal{H}i} = f_{vi} \left( \frac{\delta\rho}{\rho} \right)_{vi}. \quad (\text{A8})$$

We might demand  $\delta_{\mathcal{H}} \in \{-10^{-6}, -10^{-5}\}$ , which means we might take  $f_{vi} \in \{10^{-4}, 10^{-2}\}$ , depending on what values of  $(\delta\rho/\rho)_{vi}$  are acceptable for the nonbaryonic dark matter power spectrum.

Once values of  $h_{ri}$  and  $f_{vi}$  are specified, then by (14), (dropping the index  $w$ ),  $\bar{\gamma}_i = 1 - f_{vi} + f_{vi}h_{ri}^{-1}$ , while the initial matter density parameter,  $\bar{\Omega}_{Mi}$ , is fixed in terms of  $\bar{\gamma}_i$ ,  $\epsilon_i$  and  $f_{vi}$  by (A3). At the present epoch, the integral constraint (A3), combined with the relation for the cosmological redshift determined by wall observers,  $z + 1 = \bar{a}_0\bar{\gamma}/(\bar{a}\bar{\gamma}_0)$ , gives

$$1 - f_{v0} = \frac{(1 - \epsilon_i)\bar{\Omega}_{M0}\bar{\gamma}_i^2 f_{vi}^{2/3}\bar{\Omega}_{k0}^2}{(1 + z_i)^2 f_{v0}^{2/3} A_i^2} \quad (\text{A9})$$

where  $z_i \simeq 1100$ , and

$$A_i \equiv \frac{f_{vi}^{1/3}\bar{\Omega}_{k0}\bar{a}_i}{f_{v0}^{1/3}\bar{a}_0} = \bar{\Omega}_{M0} \left[ \frac{f_{vi}(1 - \epsilon_i)}{(1 - f_{vi})h_{ri}^2} - \epsilon_i \right], \quad (\text{A10})$$

where we have used (A4) to express  $\bar{a}_0/\bar{a}_i$  in terms of  $h_{ri}$  and other parameters in the last step. We evaluate both (A1) and (A2) at the present epoch  $t_0$  and at the time of last scattering,  $t_i$ , and compare them at each epoch to eliminate  $t_0$  and  $t_i$ . We then further eliminate  $t_\epsilon$  from the two resulting expressions to also obtain

$$\sqrt{A_i(A_i + \bar{\Omega}_{M0}\epsilon_i)} - \bar{\Omega}_{M0}\epsilon_i \ln \left( \sqrt{\frac{A_i}{\bar{\Omega}_{M0}|\epsilon_i|}} + \sqrt{\left| 1 + \frac{A_i}{\bar{\Omega}_{M0}\epsilon_i} \right|} \right) - \frac{2}{3} \sqrt{\frac{(1 - f_{vi})A_i^3}{f_{v0}(1 - \epsilon_i)f_{vi}\bar{\Omega}_{M0}}}$$

$$= \sqrt{\bar{\Omega}_{k0}(\bar{\Omega}_{k0} + \bar{\Omega}_{M0}\epsilon_i)} - \bar{\Omega}_{M0}\epsilon_i \ln \left( \sqrt{\frac{\bar{\Omega}_{k0}}{\bar{\Omega}_{M0}|\epsilon_i|}} + \sqrt{\left| 1 + \frac{\bar{\Omega}_{k0}}{\bar{\Omega}_{M0}\epsilon_i} \right|} \right) - \frac{2}{3} \sqrt{\frac{(1 - f_{v0})\bar{\Omega}_{k0}^3}{f_{v0}(1 - \epsilon_i)f_{vi}\bar{\Omega}_{M0}}} \quad (\text{A11})$$

For fixed  $z_i$ ,  $f_{vi}$  and  $h_{ri}$  the combination of eqs. (A5), (A9) and (A11) determines three of the parameters  $\{\bar{\Omega}_{M0}, \bar{\Omega}_{k0}, \epsilon_i, f_{v0}\}$ , leaving one independent parameter in addition to  $\bar{H}_0$ . Of course, the values of  $z_i$ ,  $f_{vi}$  and  $h_{ri}$  which are consistent with the observed CMB, do

vary over some small ranges. Given the existence of the tracker solution, however, these small variations do not significantly affect macroscopic cosmological parameters. The macroscopic properties of the universe depend significantly on the two independent parameters  $\bar{H}_0$  and  $f_{v0}$ .

## APPENDIX B: TRACKER SOLUTION TO THE BUCHERT EQUATIONS

As noted in ref. [15], setting  $\epsilon_i = 0$  in the general solution gives a solution which is a strong attractor in the phase space. Physically this solution represents one in which the void regions expand as empty Milne universes,  $a_v = a_{v0}t$ , where  $a_{v0} \equiv \bar{\Omega}_{k0}^{1/2} \bar{a}_0 \bar{H}_0 f_{v0}^{-1/6} f_{vi}^{-1/3}$ , and  $h_r = 2/3$ . The solution is given by

$$\bar{a} = \frac{\bar{a}_0 (3\bar{H}_0 t)^{2/3}}{2 + f_{v0}} \left[ 3f_{v0} \bar{H}_0 t + (1 - f_{v0})(2 + f_{v0}) \right]^{1/3} \quad (\text{B1})$$

$$f_v = \frac{3f_{v0} \bar{H}_0 t}{3f_{v0} \bar{H}_0 t + (1 - f_{v0})(2 + f_{v0})}, \quad (\text{B2})$$

with two independent parameters  $\bar{H}_0$  and  $f_{v0}$ .

All other quantities of interest may be determined from (B1) and (B2). For example, the parameters (18)–(20) are given by

$$\bar{\Omega}_M = \frac{4(1 - f_v)}{(2 + f_v)^2} = \frac{b(2t + 3b)}{3(t + b)^2}, \quad (\text{B3})$$

$$\bar{\Omega}_k = \frac{9f_v}{(2 + f_v)^2} = \frac{t(2t + 3b)}{2(t + b)^2}, \quad (\text{B4})$$

$$\bar{\Omega}_Q = \frac{-f_v(1 - f_v)}{(2 + f_v)^2} = \frac{-bt}{6(t + b)^2}, \quad (\text{B5})$$

where  $b = (1 - f_{v0})(2 + f_{v0})/[9f_{v0}\bar{H}_0]$ , as in (39). From (B3)–(B5) we obtain equivalent expressions for their present epoch values,  $\bar{\Omega}_{M0}$ ,  $\bar{\Omega}_{k0}$  and  $\bar{\Omega}_{Q0}$ , in terms of  $f_{v0}$  or  $t_0 = (2 + f_{v0})/(3\bar{H}_0)$ . The bare Hubble parameter, lapse function and dressed Hubble are given respectively by

$$\bar{H} = \frac{2 + f_v}{3t} = \frac{2(t + b)}{t(2t + 3b)}, \quad (\text{B6})$$

$$\bar{\gamma} = \frac{1}{2}(2 + f_v) = \frac{3(t + b)}{(2t + 3b)}, \quad (\text{B7})$$

$$H = \frac{4f_v^2 + f_v + 4}{6t} = \frac{3(2t^2 + 3bt + 2b^2)}{t(2t + 3b)^2}. \quad (\text{B8})$$

It also follows that

$$H = \frac{(4f_v^2 + f_v + 4)\bar{H}}{2(2 + f_v)} = \frac{3(2t^2 + 3bt + 2b^2)\bar{H}}{2(t + b)(2t + 3b)}. \quad (\text{B9})$$

For a number of the tests described in the paper, it is necessary to perform derivative of observational quantities with the respect to the redshift,  $z$ , as given by (38). For this purpose, a useful intermediate step is provided by

$$\frac{dt^{1/3}}{dz} = \frac{-t^{1/3}(2t + 3b)(t + b)}{3(z + 1)(2t^2 + 3bt + 2b^2)} \quad (\text{B10})$$

which follows from (38). Thus, for example, by (38), (B8) and (B10),

$$\begin{aligned} \frac{dH}{dz} &= \frac{6(t + b)(2t^3 + 3bt^2 + 6b^2t + 3b^3)}{(z + 1)t(2t^2 + 3bt + 2b^2)(2t + 3b)^2}, \quad (\text{B11}) \\ &= \frac{3f_{v0}^{1/3} \bar{H}_0 (2t^3 + 3bt^2 + 6b^2t + 3b^3)}{(2t)^{1/3} (2t^2 + 3bt + 2b^2)(2t + 3b)^{2/3}}. \end{aligned}$$

The above expressions all involve volume-average time,  $t$ . To relate them to wall time,  $\tau$ , which is assumed to be a good approximation to the time measured by typical observers in galaxies, one has to invert the relation

$$\tau = \frac{2}{3}t + \frac{4\Omega_{M0}}{27f_{v0}\bar{H}_0} \ln \left( 1 + \frac{9f_{v0}\bar{H}_0 t}{4\Omega_{M0}} \right), \quad (\text{B12})$$

where  $\Omega_{M0} = \frac{1}{2}(1 - f_{v0})(2 + f_{v0})$  is the present epoch dressed matter density.

- 
- [1] G.F.R. Ellis, in B. Bertotti, F. de Felice and A. Pascolini (eds), *General Relativity and Gravitation*, (Reidel, Dordrecht, 1984) pp. 215–288.
- [2] G.F.R. Ellis and W. Stoeger, *Class. Quantum Grav.* **4** (1987) 1697.
- [3] T. Buchert, *Gen. Relativ. Grav.* **32**, 105 (2000).
- [4] M.N. C el erier, *Astron. Astrophys.* **353**, 63 (2000); *New Adv. Phys.* **1**, 29 (2007) [astro-ph/0702416].
- [5] K. Tomita, *Mon. Not. R. Astr. Soc.* **326**, 287 (2001); *Prog. Theor. Phys.* **106**, 929 (2001).
- [6] S. R as anen, *JCAP* 02 (2004) 003.
- [7] E.W. Kolb, S. Matarrese, A. Notari and A. Riotto, *Phys. Rev. D* **71**, 023524 (2005); E.W. Kolb, S. Matarrese and A. Riotto, *New J. Phys.* **8**, 322 (2006).
- [8] J.W. Moffat, *JCAP* 10 (2005) 012; *JCAP* 05 (2006) 001.
- [9] G.F.R. Ellis and T. Buchert, *Phys. Lett. A* **347**, 38 (2005).

- [10] The Buchert equations were developed by a number of researchers in various steps. Buchert and Ehlers [76] first considered the averaging problem in Newtonian cosmology, but also concluded that an equation equivalent to (2) remained true in full general relativity. An equation equivalent to (1) was independently discussed by Carfora and Piotrkowska [77]. The set of equations (1)–(3) were then discussed in the perturbative relativistic dust case by Russ, Soffel, Kasai and B orner [78]. The properties of the full set of equations (1)–(4), in a fully non-perturbative relativistic setting, were subsequently discussed by Buchert [3] and also extended to perfect fluids [79].
- [11] An alternative scheme to that of Buchert was proposed earlier by Zalaletdinov [80], which applies to general macroscopic averages in general relativity. It averages all of the Einstein equations, and so an additional integrabil-

- ity condition is not required. However, to make contact with physical situations, such as cosmology, many additional assumptions are required [81]–[83].
- [12] Recently many new approaches have been suggested to averaging schemes – see, e.g., [84]–[89]. Our focus here is not on the details of the averaging scheme, but in the physical interpretation of average cosmological parameters when the variance in local geometry is large. Although there may be further modifications, it is hoped that since Buchert’s scheme is phenomenologically robust enough to encapsulate the leading order changes to the average evolution from the growth of density perturbations.
- [13] A. Ishibashi and R.M. Wald, *Class. Quantum Grav.* **23** (2006) 235.
- [14] D.L. Wiltshire, *New J. Phys.* **9**, 377 (2007).
- [15] D.L. Wiltshire, *Phys. Rev. Lett.* **99**, 251101 (2007).
- [16] D.L. Wiltshire, *Int. J. Mod. Phys. D* **17**, 641 (2008).
- [17] T. Buchert, J. Larena and J.M. Alimi, *Class. Quantum Grav.* **23**, 6379 (2006); J. Larena, J.M. Alimi, T. Buchert, M. Kunz and P.S. Corasaniti, arXiv:0808.1161.
- [18] S. Räsänen, *JCAP* **11** (2006) 003; *JCAP* **04** (2008) 026.
- [19] N. Li and D.J. Schwarz, *Phys. Rev. D* **76**, 083011 (2007).
- [20] N. Li and D.J. Schwarz, *Phys. Rev. D* **78**, 083531 (2008).
- [21] T. Mattsson, arXiv:0711.4264.
- [22] E. Rosenthal and E.E. Flanagan, arXiv:0809.2107.
- [23] D.L. Wiltshire, *Phys. Rev. D* **78**, 084032 (2008).
- [24] B.M. Leith, S.C.C. Ng and D.L. Wiltshire, *Astrophys. J.* **672**, L91 (2008).
- [25] A.G. Riess *et al.*, *Astrophys. J.* **659**, 98 (2007).
- [26] The detailed comparison with more recent *SneIa* data sets [55, 56] is discussed in a forthcoming paper [74].
- [27] D.L. Wiltshire, in *Dark Matter in Astroparticle and Particle Physics: Proceedings of the 6th International Heidelberg Conference*, eds H.V. Klapdor–Kleingrothaus and G.F. Lewis, (World Scientific, Singapore, 2008) pp. 565–596 [arXiv:0712.3984].
- [28] E. Komatsu *et al.*, *Astrophys. J. Suppl.* **180**, 330 (2009).
- [29] D.J. Eisenstein *et al.*, *Astrophys. J.* **633** (2005) 560; S. Cole *et al.*, *Mon. Not. R. Astr. Soc.* **362** (2005) 505.
- [30] W.J. Percival *et al.*, *Mon. Not. R. Astr. Soc.* **381**, 1053 (2007).
- [31] A. Cabré and E. Gaztañaga, *Mon. Not. R. Astr. Soc.* **393**, 1183 (2009).
- [32] V.J. Martínez *et al.*, *Astrophys. J.* **696**, L93 (2009); Erratum *ibid.* **703**, L184 (2009).
- [33] A.G. Sánchez, M. Crocce, A. Cabré, C.M. Baugh and E. Gaztañaga, *Mon. Not. R. Astr. Soc.* in press; arXiv:0901.2570.
- [34] W.J. Percival *et al.*, arXiv:0907.1660.
- [35] E.A. Kazin *et al.*, arXiv:0908.2598.
- [36] H.J. Seo *et al.*, arXiv:0910.5005.
- [37] As discussed in Sec. 10 of ref. [14], in a void-dominated universe one might expect a nearly fractal galaxy distribution below the scale of statistical homogeneity. However, this is a likely outcome of the model, rather than an input, and is limited by scale. Since no assumptions about fractals are made in the model, I have decided to rename it to avoid potential confusion. The word “timescape” captures the idea that it is the relative calibration of ideal clocks in a nonuniform dynamically evolving geometry which is a distinguishing feature of the present cosmology.
- [38] J.E. Forero–Romero, Y. Hoffman, S. Gottlöber, A. Klypin and G. Yepes, *Mon. Not. R. Astr. Soc.* **396**, 1815 (2009).
- [39] F. Hoyle and M.S. Vogeley, *Astrophys. J.* **566**, 641 (2002); *Astrophys. J.* **607**, 751 (2004).
- [40] A.V. Tikhonov and I.D. Karachentsev, *Astrophys. J.* **653**, 969 (2006).
- [41] In the standard cosmology distances are specified assuming Euclidean geometry on nearby scales. In the timescape scenario there are strong spatial curvature gradients within the scale of statistical homogeneity, and thus the Euclidean distance measure is not a good one strictly speaking. We can make contact with the usual distance scales, however, if we assume that distances are calibrated with the dressed geometry (26) beyond the scale of statistical homogeneity. Below the scale of statistical homogeneity we will quote the conventional distances used by astronomers. However, the actual calibration of distance measures below this scale is a subtle and interesting question still to be resolved.
- [42] It is of course envisaged that such a formalism will eventually be developed in terms of contrasts with respect to various average effective cosmological backgrounds. The models are simply still at an early stage of development.
- [43] A. Gabrielli, F. Sylos Labini, M. Joyce and L. Pietronero, *Statistical Physics for Cosmic Structures*, (Springer, Berlin, 2005).
- [44] D.W. Hogg, D.J. Eisenstein, M.R. Blanton, N.A. Bahcall, J. Brinkmann, J.E. Gunn and D.P. Schneider, *Astrophys. J.* **624**, 54 (2005).
- [45] F. Sylos Labini, N.L. Vasilyev, Y.V. Baryshev and M. López-Corredoira, *Astron. Astrophys.* **505**, 981 (2009).
- [46] In the notation of Buchert and Carfora [92]:  $H_{\mathcal{M}} = H_w$ ;  $H_{\mathcal{E}} = H_v$ ;  $\lambda_{\mathcal{M}} = 1 - f_v$ ;  $\mathcal{Q}_{\mathcal{M}} = 0$  or  $\delta^2 H_{\mathcal{M}} = \frac{1}{3} \langle \sigma^2 \rangle_{\mathcal{M}}$ ;  $\mathcal{Q}_{\mathcal{E}} = 0$  or  $\delta^2 H_{\mathcal{E}} = \frac{1}{3} \langle \sigma^2 \rangle_{\mathcal{E}}$ ; and  $\mathcal{Q}_{\mathcal{D}} = 6\lambda_{\mathcal{M}}(1 - \lambda_{\mathcal{M}})(H_{\mathcal{E}} - H_{\mathcal{M}})^2$ .
- [47] The best-fit values for the fit to the Riess07 data set obtained in ref. [24] were fit using the full exact solution for  $h_{ri} = 0.99999$ ,  $f_{vi} = 10^{-4}$ , and  $z_i = 1100$ . The difference in best-fit parameters values between the full solution and the tracker solution in this case turns out to be 0.1% in  $H_0$ , 1% in  $f_{v0}$ , and 3% in  $\Omega_{M0}$ . Thus the tracker solution is accurate at the precision of current tests. If higher precision is required it will also become necessary to also incorporate radiation species.
- [48] The magnitude of  $\Omega_{\mathcal{Q}}$  is of similar order to the volume-average variance of the expansion rate found by Clarkson, Ananda and Larena [87] in an independent study, using a somewhat different averaging scheme. In comparing results one should be careful to note that Clarkson *et al.* consider domain averages on spatial hypersurfaces, when determining the “variance in the Hubble rate”. Such spatial volume averages relate to our bare cosmological quantities, rather than dressed parameters. In the present scheme one finds a greater variance in the apparent Hubble flow, once one takes into account the fact that we dress parameters using rods and clocks calibrated to our local geometry whose spatial curvature differs from the spatial volume average one.
- [49] In the terminology of Kolb, Marra and Mattarese [90] (26) is a “phenomenological background solution”, whereas (22) is an “averaged background solution”.
- [50] B.E. Schaefer, *Astrophys. J.* **660**, 16 (2007); N. Liang,

- W. K. Xiao, Y. Liu and S.N. Zhang, *Astrophys. J.* **685**, 354 (2008); L. Amati, C. Guidorzi, F. Frontera, M. Della Valle, F. Finelli, R. Landi and E. Montanari, *Mon. Not. R. Astr. Soc.* **391**, 577 (2008); R. Tsutsui, T. Nakamura, D. Yonetoku, T. Murakami, Y. Kodama and K. Takahashi, *JCAP* 08 (2009) 015.
- [51] B.E. Schaefer, in preparation.
- [52] Similar discontinuous  $w(z)$  functions are found in  $\Lambda$ CDM models with a small amount of spatial curvature,  $|\Omega_{k0}| = 0.02$ , if  $w(z)$  is mistakenly reconstructed with the assumption of a spatially flat cosmology [91].
- [53] G.B. Zhao and X. Zhang, arXiv:0908.1568.
- [54] P. Serra, A. Cooray, D.E. Holz, A. Melchiorri, S. Pandolfi and D. Sarkar, arXiv:0908.3186.
- [55] M. Kowalski *et al*, *Astrophys. J.* **686**, 749 (2008).
- [56] M. Hicken *et al*, *Astrophys. J.* **700**, 1097 (2009).
- [57] R. Kessler *et al*, arXiv:0908.4274.
- [58] V. Sahni, A. Shafieloo and A.A. Starobinsky, *Phys. Rev. D* **78**, 103502 (2008).
- [59] A. Shafieloo, V. Sahni and A.A. Starobinsky, arXiv:0903.5141.
- [60] E. Gaztañaga, A. Cabré and L. Hui, *Mon. Not. R. Astr. Soc.* **399**, 1663 (2009).
- [61] C. Alcock and B. Paczyński, *Nature* **281**, 358 (1979).
- [62] A new variant of the Alcock–Paczyński diagnostic has been recently discussed by García-Bellido and T. Haugbøelle [93] in the context of LTB models.
- [63] E. Gaztañaga, A. Cabré, F. Castander, M. Crocce and P. Fosalba, *Mon. Not. R. Astr. Soc.* **399**, 801 (2009).
- [64] The value of  $\Omega_{B0}$  has been determined assuming a tight range of values for the baryon-to-photon ratio at decoupling,  $\eta_{B\gamma} = 4.6\text{--}5.6 \times 10^{-10}$ , as would be consistent with primordial lithium abundance observations. The relatively large uncertainties here reflect the  $1\sigma$  uncertainties in  $\Omega_{M0}$  which is not tightly constrained by Snela. Allowing a wider range of values for  $\eta_{B\gamma}$  would further increase the uncertainty in  $\Omega_{B0}$ . The estimates of  $\Omega_{M0}$  and  $\Omega_{B0}$  are coupled, and this has been taken into account in determining  $\Omega_{C0}/\Omega_{B0}$ .
- [65] C. Clarkson, B. Bassett and T.C. Lu, *Phys. Rev. Lett.* **101**, 011301 (2008).
- [66] S. February, J. Larena, M. Smith and C. Clarkson, arXiv:0909.1479.
- [67] A. Sandage, *Astrophys. J.* **136**, 319 (1962); G.C. McVittie, *Astrophys. J.* **136**, 334 (1962); A. Loeb, *Astrophys. J.* **499**, L111 (1998).
- [68] J.P. Uzan, C. Clarkson and G.F.R. Ellis, *Phys. Rev. Lett.* **100**, 191303 (2008).
- [69] P.S. Corasaniti, D. Huterer and A. Melchiorri, *Phys. Rev. D* **75**, 062001 (2007); J. Liske *et al.*, *Mon. Not. R. Astr. Soc.* **386**, 1192 (2008).
- [70] A.G. Riess *et al.*, *Astrophys. J.* **699**, 539 (2009).
- [71] M.J. Reid, J.A. Braatz, J.J. Condon, L.J. Greenhill, C. Henkel and K.Y. Lo, *Astrophys. J.* **695**, 287 (2009).
- [72] The first distance of  $49.5 \pm 7.5$  Mpc, announced at <http://www.nrao.edu/pr/2009/megamaser/>, to galaxy UGC 3789 with a recession velocity of  $3325 \text{ km sec}^{-1}$  [71], would represents a value  $H_0 \simeq 67.2 \pm 11.4 \text{ km sec}^{-1} \text{ Mpc}^{-1}$ , though this would change with Hubble flow modelling (J.A. Braatz, private communication). UGC 3789 happens to be close to the distance scale at which we expect a peak in the average  $H_0$ , but also the maximum variance.
- [73] J. Kwan, M.J. Francis and G.F. Lewis, arXiv:0902.4249.
- [74] P.R. Smale and D.L. Wiltshire, in preparation.
- [75] Buchert and Carfora [92] refer to the same approximation as a “three-scale model”, as they count the scale of statistical homogeneity as one of the scales. My two scales refer to largest relevant scales in the “nonlinear regime”.
- [76] T. Buchert and J. Ehlers, *Astron. Astrophys.* **320**, 1 (1997); J. Ehlers and T. Buchert, *Gen. Relativ. Grav.* **29**, 733 (1997).
- [77] M. Carfora and K. Piotrkowska, *Phys. Rev. D* **52**, 4393 (1995).
- [78] H. Russ, M.H. Soffel, M. Kasai and G. Börner, *Phys. Rev. D* **56**, 2044 (1997).
- [79] T. Buchert, *Gen. Relativ. Grav.* **33**, 1381 (2001).
- [80] R.M. Zalaletdinov, *Gen. Relativ. Grav.* **24**, 1015 (1992); **25**, 673 (1993).
- [81] A.A. Coley, N. Pelavas and R.M. Zalaletdinov, *Phys. Rev. Lett.* **95**, 151102 (2005).
- [82] R.J. van den Hoogen, *J. Math. Phys.* **50**, 082503 (2009).
- [83] A. Paranjape and T.P. Singh, *Phys. Rev. D* **76**, 044006 (2007); A. Paranjape, *Phys. Rev. D* **78**, 063522 (2008).
- [84] R.A. Sussman, arXiv:0809.3314.
- [85] J. Larena, *Phys. Rev. D* **79**, 084006 (2009).
- [86] I.A. Brown, J. Behrend and K.A. Malik, arXiv:0903.3264.
- [87] C. Clarkson, K. Ananda and J. Larena, *Phys. Rev. D* **80**, 083525 (2009).
- [88] A.A. Coley, arXiv:0908.4281.
- [89] M. Korzyński, arXiv:0908.4593.
- [90] E.W. Kolb, V. Marra and S. Matarrese, arXiv:0901.4566.
- [91] G. Barenboim, E. Fernández-Martínez, O. Mena and L. Verde, arXiv:0910.0252.
- [92] T. Buchert and M. Carfora, *Class. Quantum Grav.* **25**, 195001 (2008).
- [93] J. García-Bellido and T. Haugbøelle, *JCAP* 09 (2009) 028.